April 2009

Modeling and Measuring Nasal Airflow Characteristics

Karen Lynne Krasko
Worcester Polytechnic Institute

Lincoln Edward Barber
Worcester Polytechnic Institute

Robert D. Lowry
Worcester Polytechnic Institute

Modeling and Measuring Nasal Airflow Characteristics

Lincoln Barber

Karen Krasko

Rob Lowry

Modeling and Measuring Nasal Airflow Characteristics

Project number – see format for BE. Unclear if that cover sheet is more than a page?

A proposal for Major Qualifying Project
Submitted to the Faculty of
WORCESTER POLYTECHNIC INSTITUTE
in partial fulfillment of the requirements for the
Degree of Bachelor of Science

By:

Lincoln Barber
Karen Krasko
Rob Lowry

Date:
October 18, 2008

Report Submitted to

Professor Brian Savilonis
Worcester Polytechnic Institute

TABLE OF CONTENTS

AUTHORSHIP PAGE

Introduction	Karen and Rob
Literary Review	
Nasal Anatomy and Function	Karen
Nasal Turbinectomy	Karen
Previous Studies	Lincoln
Basic Fluid Dynamics	Rob
Summary	Karen
Project Approach	Karen
Project Hypothesis	Karen and Rob
Project Assumption	Rob
Project Specifications	Karen
Design	Karen
Clarification of Design Goals	Karen
Objectives	Karen
Development of Revised Client Statement	Rob
Conceptual Designs	Lincoln and Rob
Preliminary Designs	Karen
Appendix A	Rob

Acknowledgements

The team would like to sincerely thank the following individuals for their contributions to the project.

Bradley A Miller and Kenneth A. Stafford of the Robotics Department—For their contributions in motor control

Barbara L. Furhman, WPI Mechanical Engineering Department—For her assistance in obtaining supplies to the group

Neil Whitehouse, WPI Machinist – For his continuous help and support in the machine shop

Sergey N. Makarov, WPI Electrical and Computer Engineering Department—for supplying the group with equipment

Brian James Savilonis, advisor, WPI Mechanical Engineering Department--

Abstract

Studies have shown that millions of Americans suffer from some form of chronic rhinitis. To fix this problem surgeons perform what is called a partial nasal turbinectomy, which currently may improve the patient's condition or lead to an iatrogenic condition called Empty Nose Syndrome. This surgery has previously been evaluated through reported patient perceptions of its success, through computer simulation, and limited steady state flow *In vitro* studies. The goal of the project is to design and construct a machine that is able to control tidal volumes and respiration rates so one can explore various breathing patterns for any age or possible physical activity level. The machine will allow the team to analyze various unsteady state nasal flow patterns. Experiments were conducted on a 2X rigid plastic model nasal cavity to measure the pressure and airflow rate in the nose before and after a nasal turbinectomy. The data will help verify computational calculations and enhance the understanding of a proper turbinate alteration.

TABLE OF FIGURES

TABLE OF TABLES

CHAPTER 1: INTRODUCTION

Chronic rhinitis adversely affects 20 million Americans [1] and cost United States' employers more than 250 million dollars in 1998 [2]. Rhinitis is a very common condition and may be defined as inflammation of the inner lining of the nose. Symptoms include rhinorrhea, or runny nose, nasal itching, nasal congestion and sneezing. This affliction can be either acute or chronic, and may be brought on by allergic sensitivity. Rhinitis adversely effects breathing as well. Both prescription and over the counter medications can provide relief, but many sufferers need a more aggressive treatment. To improve breathing, many people undergo a surgery called a nasal turbinectomy.

A nasal turbinectomy is the reduction or removal of a turbinate bone and/or cartilage that is located in the nose. The turbinate bone is situated along the side wall of the nasal cavity, and is covered by mucous membrane [3]. This structure helps direct air through the nose allowing it to be properly acclimated on its way to the lungs. By the surgeon removing part of the bone and tissue, the passage for airflow is increased and the patient is able to breathe better. However, a nasal turbinectomy is performed solely on the judgment of the surgeon because there is very little information about the effects of this surgery in literature. Post turbinectomy patients often experience an increase in air flow through the nose. However, a common side effect is that the airflow patterns inside the nasal cavity are altered in a negative way, disturbing the nasal passage's ability to control breath temperature and humidity before entering the lungs [4].

There have been many studies conducted to better understand the effects of nasal turbinectomies. Most experiments that have been conducted have been based on patient perception, computational fluid dynamic models and *in vitro* experiments. These results lack quantitative data and need to be improved. However, two different studies in 2007 and 2008 were conducted by two teams of students at Worcester Polytechnic Institute [5], [6].

Experiments were conducted on a 2X rigid plastic model nose to measure the pressure and air flow rate in the nose before and after a nasal turbinectomy. It was concluded that the flow inside the nasal cavity cannot be modeled with a quasi-steady flow because separated flow patterns inside the nose may not develop at the same rate as with variable flow. In both experiments, the pressure data has also been inconclusive because of significant noise generated from the motor which affected pressure sensors.

The goal of this project is to conduct further research on the effects of nasal turbinectomies and to address the gap by measuring quantitative data to better understand breathing. By designing and constructing a device to stimulate breathing, pressure and airflow data will be obtained. There are four main goals of this project;

- Construct a device that replicates scaled human breathing
- Model and measure the pressure drop versus the air flow at various breathing rates
    i. Reduce signal noise from lung function
- Observe pressure differential before and after the surgery

The data will help verify computational calculations and enhance the understanding of a proper turbinate alteration, reducing the overall number of patients with unwanted side effects from the surgery. Instead of surgeons having to perform based on judgment, they will have quantitative data to assist in an ideal nasal turbinectomy.

CHAPTER 2: LITERARY REVIEW

The following chapter discusses nasal anatomy and functions, the process of a nasal turbinectomy, previous studies regarding nasal turbinectomies, and the elements of fluid dynamics that are relevant to this project. Understanding the human nose and related studies will be valuable in designing, testing and analyzing the model of the nasal cavities.

NASAL ANATOMY AND FUNCTION

The nasal cavity is located in the nose and functions as a passageway for airflow during respiration as well as containing the organs for smell. The cavity is primarily used during at-rest respiration. In active respiration, the airflow volume increases because the mouth is opened which routes the air away from the nose. Within the nasal cavity, air is either warmed or cooled to within 1 degree of body temperature before joining the back of the throat and the trachea. Also, the nasal cavity is important because air is humidified and dust and particles are removed by cilia. The focus of this research will be the structures within the nasal cavity and how they influence the airflow.

The nasal cavity begins at the tip of your nose and ends where the cavity meets the throat. The nasal septum which is composed of cartilage, divides the cavity down the middle into two sections for airway. In the cavity, there is variability in the surfaces composed of bone, tissue and hair which can cause swirling and affect airflow.

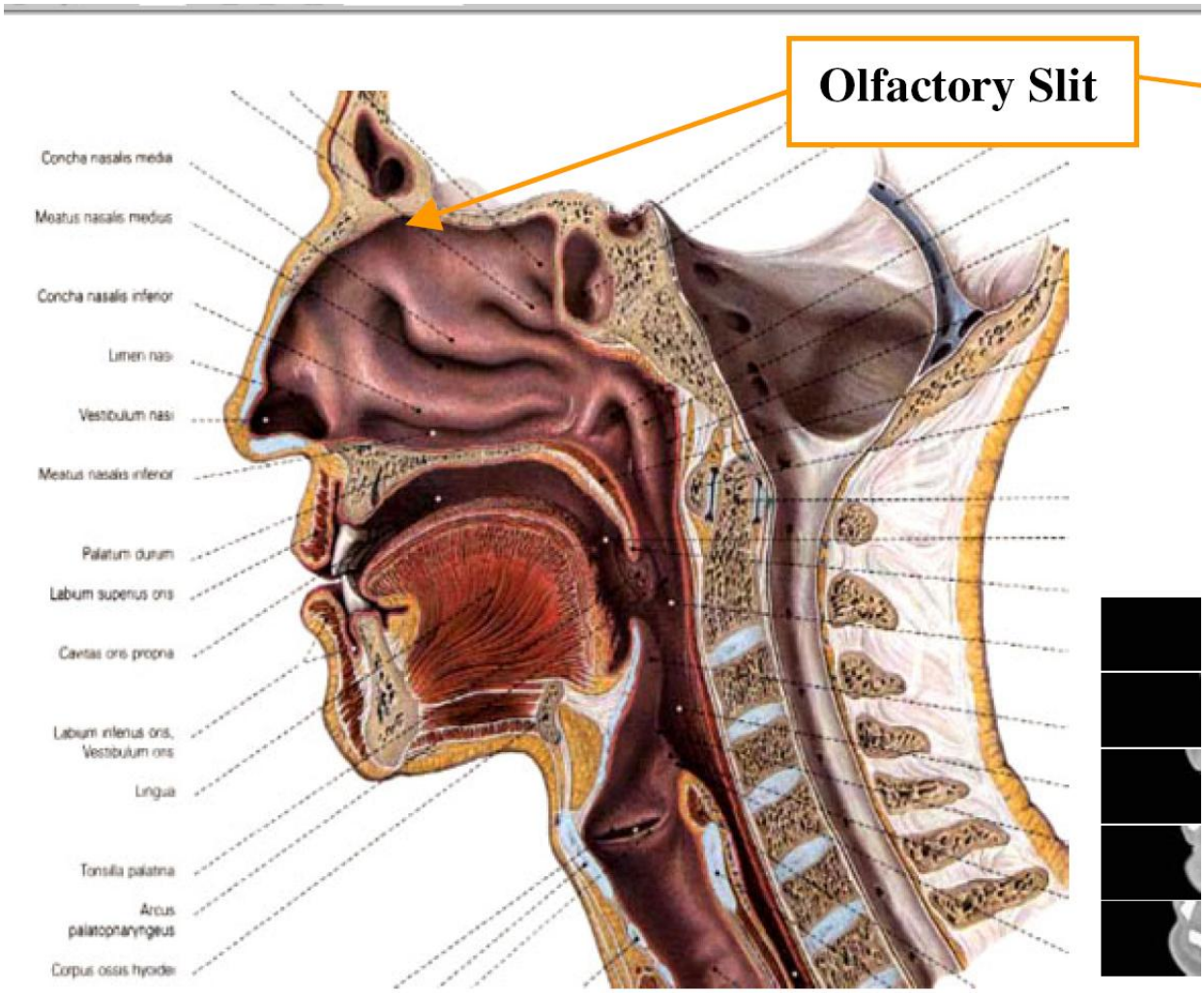

Figure 1: Nasal Cavity [7]

Within the cavity there are four nasal valves or flow limiting segments: external valve, internal valve, septal valve and inferior turbinates [8]. The cross section area of the nasal cavity slowly decreases throughout the nasal valves until the internal valve, where the cross-section is different then the rest of the cavity. This section contains three horizontal outgrowths called turbinates, which are located on the sides of the nasal cavity. The three outgrowths are called the inferior, middle and superior turbinates as seen in Figure 2~~Figure 2~~ below:

Formatte
Roman, 12

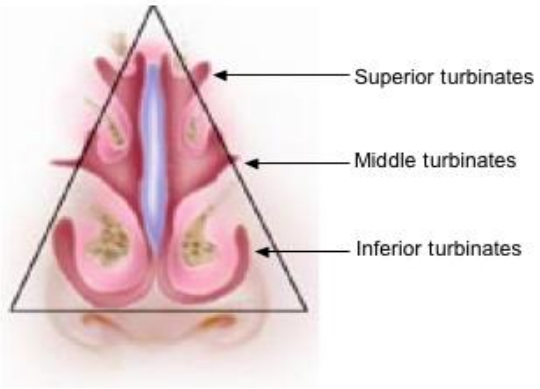

Figure 2: Turbinates [9]

The varying cross-sectional areas of these turbinates contribute to the complexity of airflow through the nasal cavity. The dimensions of the nasal cavity in the turbinate area are about 40 mm high, 1-3 mm wide, and approximately 60 mm deep [10].

After the inferior turbinate, the airflow rejoins into one stream and enters the final region of the nasal cavity called the nasopharynx and continues into the pharynx or part of the throat. Because the cross-sectional area of the nasal cavity in the nasopharynx is greater than in the turbinates, it is not the cause of airflow restrictions.

BREATHING RATES AND FLOW

To properly mimic human breathing, several functional measurements must be replicated accurately. The parameters of the lungs relevant to this experiment are the total volume, breathing frequency, tidal volume, volumetric flow rate and pressure. Total volume is the maximum of the tidal volume curve which relates the volume of air contained in the lungs to time over one breath. The volumetric flow rate is the negative of the first time derivative of the lung tidal volume. The sign convention is based on the choice of air flowing out of the nose to be positive. Pressure is simply the fluid pressure inside the nasal cavity. The three time dependent quantities for a healthy adult are graphically represented in

Formatte
Roman, 12

~~Figure 3~~.

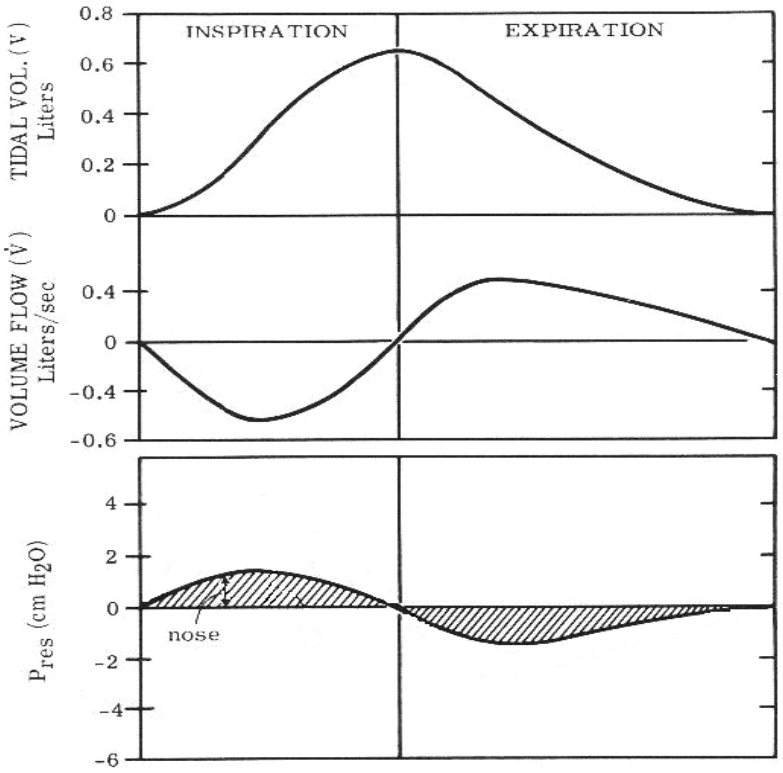

Figure 3: volume versus time, volumetric flow rate, and pressure charts [11]

Breathing rates depend on the size of the individual and are measured in breaths per minute.

Formatte

Formatte
Roman, 12

Formatte
Double, Ke

Table 1: Typical Breathing Rates cs. Age Group [11]

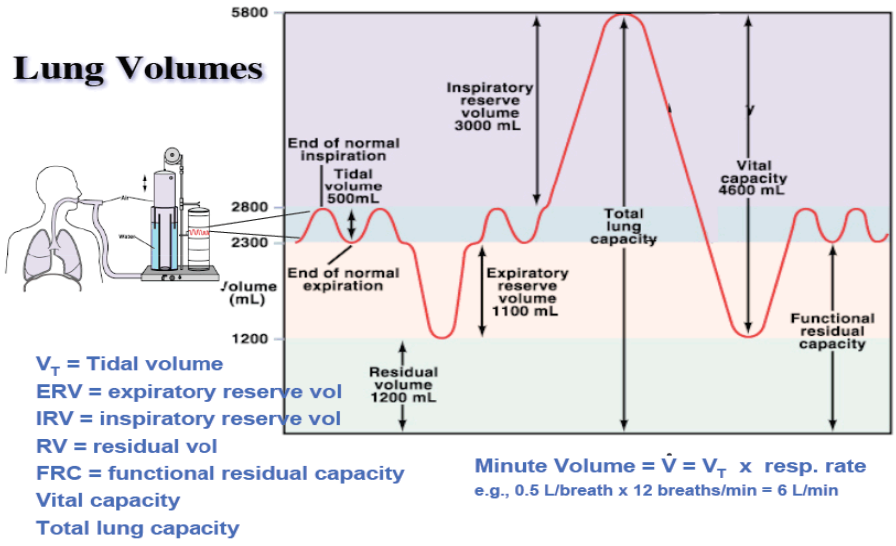

Figure 4: Lung Volumes over Breathing Cycle [12]

~~Table 1~~ gives the typical range of breathing rates broken down into age groups.

Typical Breathing Rates		
	Low (BPM)	High (BPM)
Adult	12	20
Teenager	16	25
Preschool	20	30
Infants	20	40
Newborns	44	

Table 1: Typical Breathing Rates cs. Age Group [11]

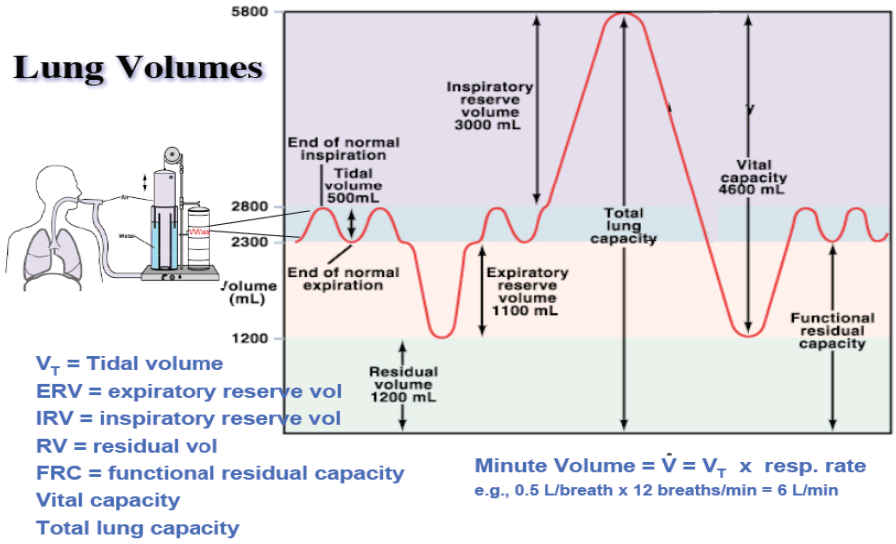

Figure 4: Lung Volumes over Breathing Cycle [12]

The total lung volume is an important quantity and correlates to the product of the piston cross sectional area and the overall piston displacement; **Error! Reference source not found.**~~Figure 4~~ illustrates typical lung volumes for the adult age group. From Figure 4 shown below, the normal lung capacity was found to vary from approximately 2.3 to 2.8 liters of air, resulting in a tidal volume of approximately 0.5 liters. The predicted tidal volumes for different breathing frequencies and weights can be inferred from Figure 5.

The basal tidal volume, or minimum tidal volume at rest, can be determined using Figure 5. The predicted tidal volume can be found from body weight and breathing frequency. Connect the body weight and breathing frequency with a straight line, and the intersection with the predicted tidal volume curve is the basal tidal volume.

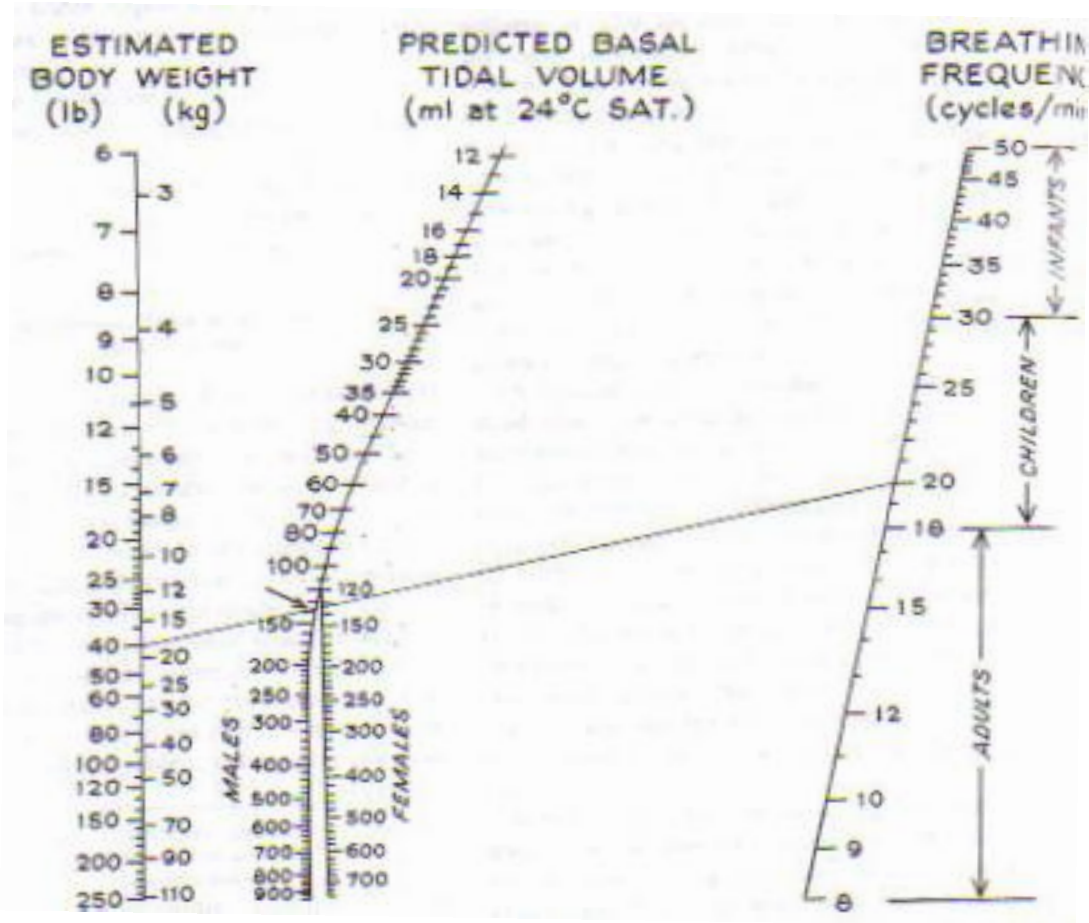

Figure 5: Radford Nomogram for predicting Basal Tidal Volume[13]

The age groups from Table 1 were used and for each group, corresponding average weights were calculated independent of gender [ref]. Figure 5 was used to determine the tidal volumes for each weight. The resulting average weights and corresponding tidal volumes were combined with Table 1 and are shown in Table 2.

Typical Breathing Characteristics				
	Weight [lb]	**Breathing Rate Low [BPM]**	**Breathing Rate High [BPM]**	**Predicted Tidal Volume [L]**
Adult	180	12	20	.4-.5
Teenager (14yr)	115	16	25	.24-.3
Preschool (4yr)	36	20	30	.09-.12
Infants (1yr)	22	20	40	.06-.08
Newborns (>1m)	7.5	44	44	.02

Table 2: SUMMERY OF BREATHING CHARACTERISTICS

Once a comprehensive understanding of the physical parameters of breathing is developed into mathematical equations, an accurate model can be developed. These equations will be critical down the road for altering the situation to benefit scientists and engineers without loss of accuracy. These parameters are represented by two age dependent values and three functions of time that will differ with age as well.

NASAL TURBINECTOMY

A turbinectomy is a nasal surgery to remove part of the turbinate structures (both bone and soft tissue) in the nasal cavity [14]. The turbinates can swell and become enlarged due to trauma, severe allergies or infection, resulting in inability to breathe through the nose. Turbinectomy is performed to open up the nasal airway and improve breathing by removing some or all of the turbinates. It is a safe and effective procedure to relieve complaints of nasal stuffiness, snoring and difficult breathing [15]. These surgeries are performed under local or general anesthesia. The anatomy of the nose influences the surgeon whether only bone should be removed, or both bone and soft tissue. This may be achieved by cauterization, electrocautery, or microdebrider [16].

A microdebrider is a tiny, high-speed device that shaves soft tissue [16]. A tiny incision is made in the nose and the microdebrider is inserted through a tube into the turbinate. A computer tomography (CT) guided imaging system is used to assist the surgeon in clearly viewing the surgical site. Once inserted, the microdebrider quickly and accurately removes the desired tissue, leaving adjacent tissues intact [16]. While the surgeries themselves are very exact and done with high precision tools there is still no way to know exactly what needs to be removed for a proper turbinectomy.

PREVIOUS STUDIES

BASIC FLUID DYNAMICS

The topic of this section is an understanding of flow separation, laminar versus turbulent flow, and the necessary flow parameters, which are integral to understanding what is happening mathematically inside the nasal cavity.

Similar to all fluid flow, air flowing through the nasal passages follows the path of least resistance. When air passes through the passages of the nose, some comes in contact with the walls of the passage or other obstructions and looses speed. The air particles close to the walls of the nose have a significantly reduced speed as compared to the core of the flow stream, which creates a boundary layer. Flow separation will occur in the presence of an adverse pressure gradient across this boundary layer. This effect gives rise to vortices in the flow. See Figure 6: Laminar vs. Turbulent Flow~~Figure 5: Laminar vs. Turbulent Flow~~:

Formatte
Roman, 12

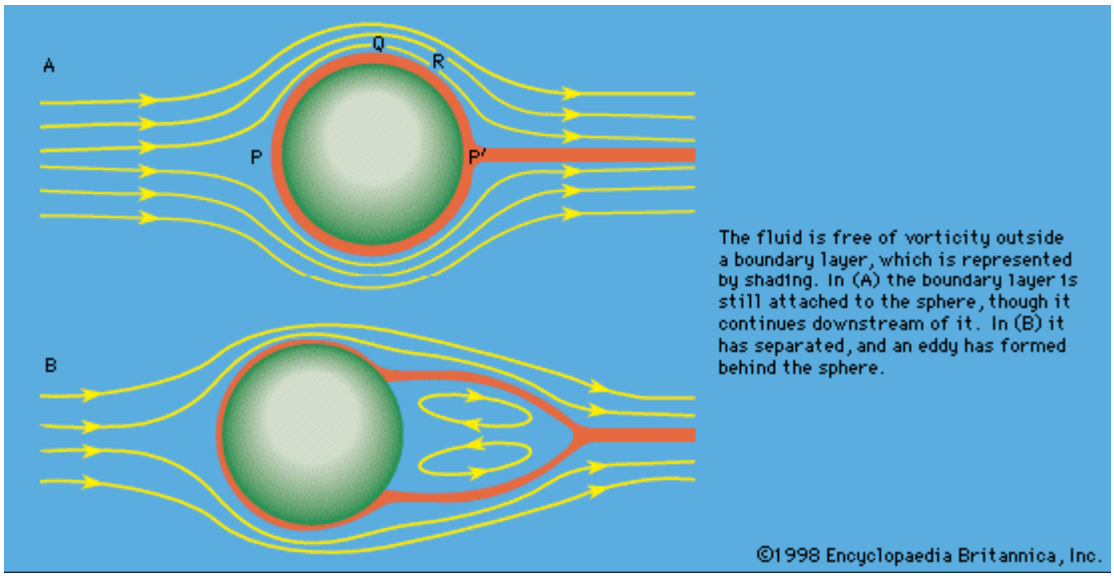

Figure 6: Laminar vs. Turbulent Flow

There are two categories of characteristic flow, laminar and turbulent. Laminar flow is characterized by smooth layers that travel with similar velocity vectors that do not frequently mix, similar to cars on a highway. Turbulent flow consists of fluid particles that mix rapidly due to chaotic changes in flow velocity, similar to a rapid river. Turbulent flow is associated with higher resistance, but is redeemed by higher flux and greater heat transfer.

When beginning to quantify parameters of fluid flow, two quantities are especially important for increasing design possibilities and reducing complications; The Reynolds number, and the Womersley number.

The Reynolds number is a dimensionless parameter defined by the ratio of dynamic pressure ($\rho u2$) and shearing stress ($\mu u / L$). This expression allows for accurate comparison of experiment parameters whether using water or air. The speed and type of fluid can easily be switched for more favorable fluids, all while maintaining accuracy. Using the parameters of the human respiratory system, the Reynolds number can be used to find the appropriate flow rate for

a model of different size that may breathe a fluid other than air. The Reynolds number is given by

$$Re_L = \frac{\rho VL}{\mu} = \frac{VL}{v}$$

Symbol	Definition	SI Units
V	Mean fluid velocity	m/s
L	Characteristic length	m
μ	Dynamic Viscosity	$N{\cdot}s/m^2$
v	Kinematic Viscosity	m^2/s
ρ	Fluid Density	kg/m^3

The Womersley Number is also used to compare experimental fluid flow properties between cases, specifically for biomechanics. This expression adjusts the pulsed flow frequency in relation to viscous effects. The Womersley number is given by:

$$\alpha = R * \sqrt{\frac{\omega}{v}},$$

where R is an appropriate length scale (for example the radius of an air way), ω is the angular frequency of the oscillations, and ν, is the kinematic viscosity of the fluid. This expression allows for the frequency of breathing to be accurately adjusted for a model of different scale that may breathe a fluid other than air. With the Reynolds and Womersley numbers, an accurate scale model of the human respiratory system can be created using any fluid.

SUMMARY

The information presented in this chapter is an overview of the necessary information required to have a full understanding of the project. The focus points that were outlined in this chapter include: the basic physiological anatomy of the human nose, the normal breathing cycle,

previous studies, and basic fluid dynamics that have previously been used to analyze the pressure and flow characteristics of the human nose.

CHAPTER 3: PROJECT APPROACH

Once the background information is thoroughly researched and understood, the design team can begin to focus on the specified project. The first steps to engage in are defining the problem, assumptions, specifications and goals. This will help to define the project as a whole and the expected outcome of a successful design.

PROJECT HYPOTHESIS

Based on an analysis of prior research, the aim of this project is to simulate unsteady flow in the nasal passages and generate a pressure versus flow rate curve. The design team will generate a pressure versus time and a flow rate versus time curve and combine them parametrically. This curve will be created for pre and post turbinectomy to determine if the surgery decreases the pressure needed to achieve a given flow rate. The team will design a mechanism that will breathe both air and water. We will utilize air analysis to quickly determine the effectiveness of the surgery being analyzed through the pressure drop across the nose.

PROJECT ASSUMPTIONS

It is well known that the viscosity of a fluid is dependent on temperature. The range of temperatures the fluid being breathed will experience is 25 C˚ to 35 C˚. For simplicity, it will be assumed that the temperature and moister content of air is constant during breathing. In normal humans breathing, air being exhaled contains more carbon dioxide; it will be assumed that the chemical composition during the course of normal breathing is constant.

It is assumed that the breathing that will be scaled is that of a person who is breathing about 10 breaths per minute and with a tidal volume of 0.5L. This volume and breathing rate

will be linearly scaled to approximate individuals of different sizes. This corresponds to an average volumetric flow rate of 5 liters per minute. It was assumed that the density of air is approximately 1.19 kg/m^3 and the viscosity of air is$1.5 \times 10^{-5}\ m^2/s$. It was also assumed that the density of water is approximately 1000 kg/m^3 and the viscosity of water is $9.8 \times 10^{-7}\ m^2/s$.

PROJECT SPECIFICATIONS

1. A model nose that represents the human nasal cavity pre- and post-operation
2. Induced flow scaled to accurately depict the human breathing flow rate and frequency
3. Pressure measurements must be obtained from the mechanism
4. A fluid that can visualize the flow patterns through the nasal cavity
5. The parts of the mechanism must be manufacturable and durable
6. The device must be user friendly and the experiment must be easily reproduced.

CHAPTER 4: DESIGN

This section will focus on the process of developing a mechanism that mimics the actual human breathing cycle to create flow through a model nose. Before we proceed with the design process, it is important to clarify the outcome of the project for the stakeholders. The three main groups of stakeholders involved are the clients, the designers, and the users. The client is the person or group of people who wants the specific project designed. The client provides the initial statement that outlines the ultimate goal of the project which motivates the designers to complete the project. The designers' job is to develop and analyze a final design and specifications so the mechanism can be easily manufactured and used in its perspective field. The final stakeholder is the user who will be operating the mechanism.

For the automated breathing mechanism, Professor Brian Savilonis is the client, Lincoln Barber, Karen Krasko and Robert Lowry are the designers and the users consist of otolaryngologists or ear nose and throat surgeons who will be using the mechanism to assist in the operation.

The design process is a step-by-step procedure that is essential to follow in order to have a successful final design. The process begins with the initial client statement. At this stage, it is crucial for the designers to clarify all of the objectives, constraints and functions in order to revise the client statement into a more concise and accurate description of the problem statement. After revising the client statement, the design phases begin. The first phase is the conceptual design where the design specifications are established and design alternatives are generated. The next phase is preliminary design where the conceptual design ideas are analyzed and evaluated in order to select the best working mechanism for the problem. In the final phase of the design process, detailed design, is where the selected design is refined and optimized in order to produce the final product.

CLARIFICATION OF DESIGN GOALS

To design an optimal system, a thorough understanding of the clients' and users' needs and requirements is required. The end product should meet the needs of the clients, while considering the constraints and wants of the designers and the users. The design team attempted to find a solution that would meet the objectives, functions and constraints defined by the stakeholders. The initial problem statement provide to the design team was:

"**Develop a mechanism that replicates the human breathing cycle to analyze fluid flow and pressure change through a model nose pre- and post- nasal turbinectomy.**"

Next, the most important goal was to qualitatively identify the requirements of the project. The design team formed a list of attributes for the design including objectives, functions and constraints. The objectives are the goals of the mechanism that the stakeholders created, the functions are the requirements that the mechanism must perform and the constraints are limitations that are applied to the design of the device. Shown below is Table ~~Table 2~~check that lists the attributes.

Formatte
Roman, 12

Objectives	Functions	Constraints
-Low noise and vibration -Cost -Accuracy -Visualization -Durability -User Friendly	-Measures pressure before and after nasal cavity -Measures flow rate before and after nasal cavity -Device can breathe both air and water -User can control and adjust parameters	-Budget -Reliability - Semi-portable - Time -Durability

Table 3: List of Attributes

OBJECTIVES

The objectives the design team brainstormed were low noise and vibration, cost effectiveness, accuracy, visualization, durability and user friendliness. However, some of these objectives are more important than others. A pairwise comparison chart was constructed to rank the design objectives in terms of their perceived relative importance. A pairwise comparison chart allows each objective to be compared with every other objective one by one. For each comparison, a value of 0, 1 or ½ is assigned. A 0 means that the objective at the start of the row is less important than the objective at the top of the column. In contrast, a 1 means the row objective is more important, while a ½ means that the two objectives are equally important. The scores for each objective are determined by simply adding across each row. The objective with the highest total has the highest rank, meaning it is the most important to focus on in the design process. Table 4 below contains the pairwise comparison chart. The relative weight of each

objective was determined by dividing the total of each objective by the summed totals of all the objectives. For example, low signal noise objective received a relative weight of: (4 / 15) x 100 = 26.67%. The weighted percent for each objective is shown in the last row of the pairwise comparison chart, shown in Table 4.

Evaluation of Design Objectives								
	Low signal noise	**Cost**	**BFR accuracy**	**Visual**	**Durable**	**User friendly**	**Total** Σ = 15	**Rank**
Low signal noise	X	1	0	1	1	1	4.0	2
Cost	0	X	0	1	1/2	1/2	2.0	3.5
Breathing flow rate accuracy	1	1	X	1	1	1	5.0	1
Visualization	0	0	0	X	0	1/2	0.5	6
Durability	0	½	0	1	X	1/2	2.0	3.5
User friendly	0	1/2	0	1/2	1/2	X	1.5	5
Relative Weight	26.67%	13.33 %	33.33 %	3.33%	23.33%	10.00%	100 %	

Table 4: Design Objectives Comparison

By observing the pairwise comparison chart, it was determined that breathing flow rate accuracy was the most important objective, followed by low signal noise, durability, cost effectiveness and then user friendliness as the least important objective. Breathing flow rate accuracy is the most important design objective because without an accurate representation of normal breathing we will be unable to obtain data to prove or disprove the theory that laminar flow is inside the nasal cavity. Since the ability to obtain this data also depends upon a clear pressure reading our second most important objective was to have low signal noise produced by the mechanical vibrations of our volume control. After these two main goals durability cost effectiveness were tied showing that the ideal design would provide a balance between these two objectives. Finally, it was decided that the ease of use was unimportant because the design team would be performing the experiments.

DEVELOPMENT OF REVISED CLIENT STATEMENT

The pairwise comparison chart was very valuable in gaining quantitative confirmation of the clients' needs and interests. With the aforementioned weighted objectives in mind, a revised client statement was created to further clarify the goal of the project. The revised client statement states:

> **"Develop and test a machine to replicate human breathing of all aged individuals and allow for accurate qualitative and quantitative evaluations of fluid flow and pressure change through a double scale nasal passage model pre- and post-nasal turbinectomy."**

CONCEPTUAL DESIGNS

After thoroughly understanding the scope of the problem we needed to construct a machine to simulate unsteady state breathing which we could visualize in our model nose. To do this we brainstormed several conceptual designs.

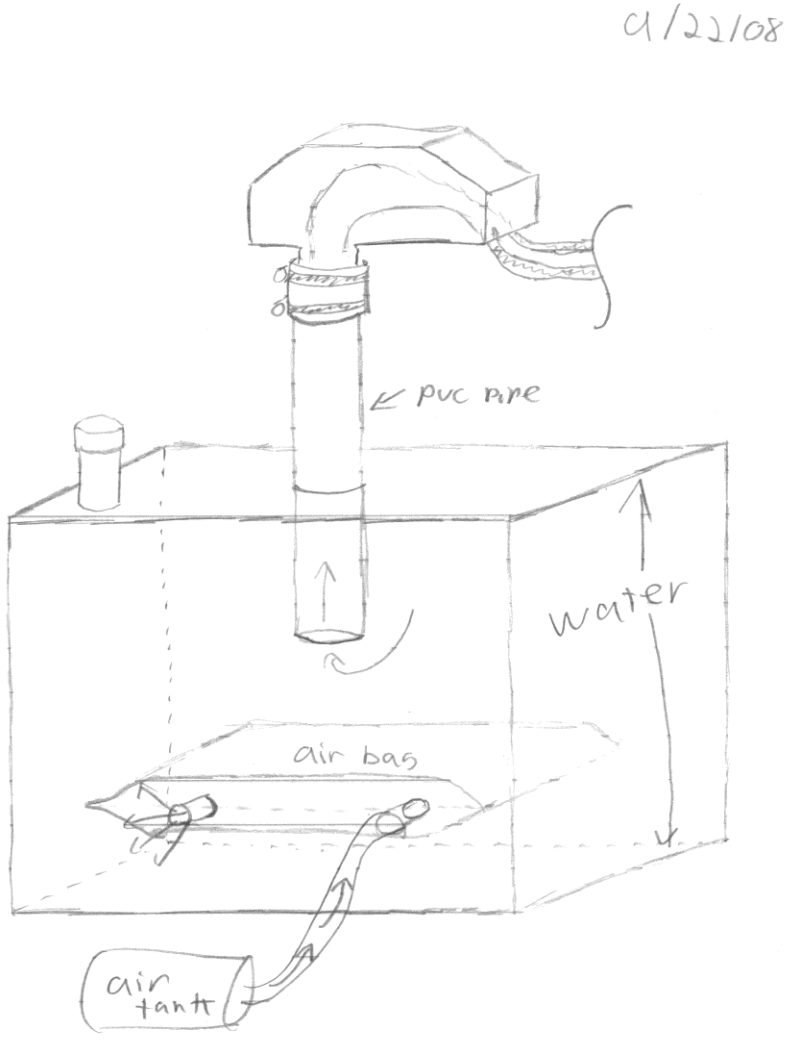

Figure 7: Pressurized Fish Tank

In this conceptual design (Figure 7), the nose is attached to a neck of PVC pipe descending down into the tank. Water is placed in the tank up to two inches from the bottom of the neck if breathing air, or to the very top of the inlet valve seen on the front right of top of the tank if breathing water. A rectangular air bag is submerged in the water at all times, and can be inflated with a solenoid valve connected to a high pressure air tank or deflated with a second solenoid valve using the weight of the water above. Opaque particles can be injected into the vinyl tubing for visualization seen in the upper right of the drawing.

Pneumatic Piston Oscillator

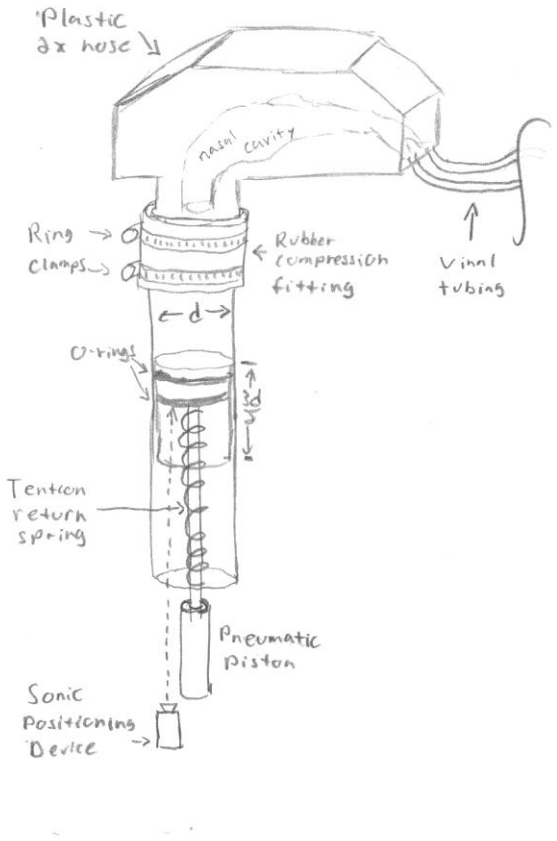

Figure 8: Pneumatic Piston Oscillator

In this design (Figure 8), the nose is attached to a neck of PVC pipe which is used as a piston chamber. A long piston with two lubricated rubber o-rings is pushed up through the piston chamber by a pneumatic piston, and returns with the help of a tension spring. A sonic positioning device measures the distance from a reference point to a point on the piston to control the flow and flow rate. This device could breathe air or water. Particles could be injected for visualization into the vinyl tubing shown in the upper right of the drawing.

Air Pressure Controlled Flow Rate

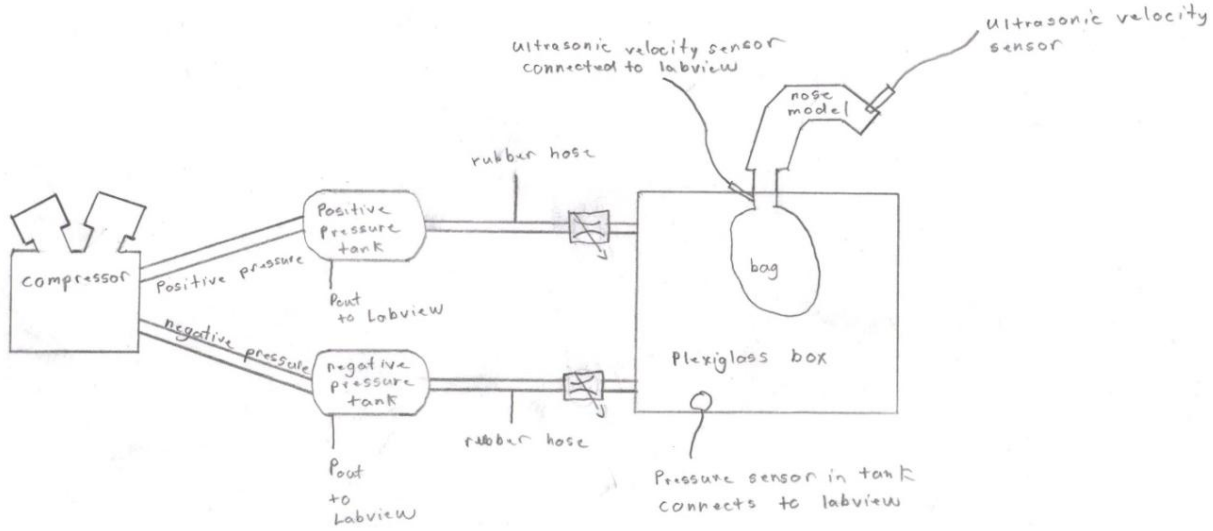

Figure 9: Air Pressure Controlled Flow Rate

Using a pressurized tank (Figure 9) and vacuum tank along with two electronically controlled solenoid valves, this design changes the volume of air inside the bag by adjusting the flow rate of air into and out of the Plexiglas box. While this design can accurately recreate a human breathing pattern it requires the ability to take real time pressure readings in multiple

places to control the solenoid valves. The overall complexity of the design and its ability to only work with air makes it less appealing than others that the design team came up with.

Linearly Controlled Piston

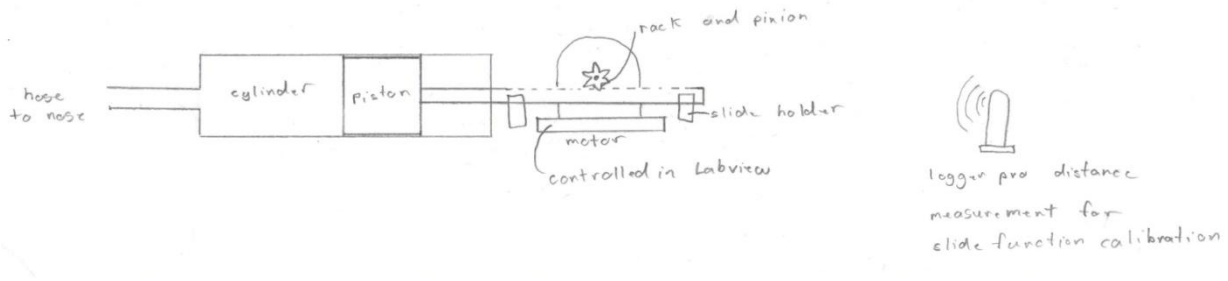

Figure 10: Linearly Controlled Piston

This design (Figure 10) shows a computer controlled Brushless DC servomotor to position a piston providing direct control of the volumetric flow rate of a test medium assuming the cross sectional area of the piston is known. This allows for excellent accuracy of the control of flow rate but the direct connection of the piston to the nose could cause too much signal noise in the pressure sensor readings. This idea was the first step in what ended up being our final design.

Linearly Controlled Piston With Model Lung

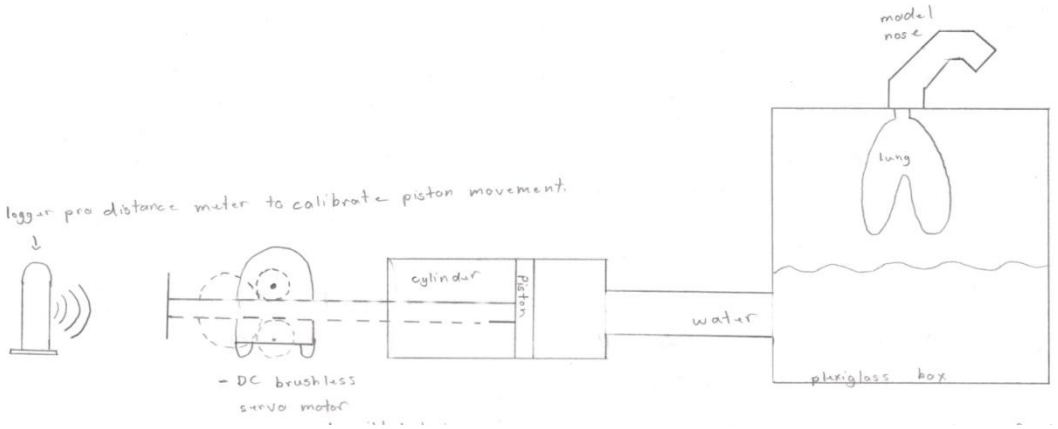

Figure 11: Linearly Controlled Piston with Model Lung

This design (Figure 11) utilizes a Brushless DC servomotor controlled through a computer to position a piston providing direct control of the volume of water inside the box pictured above. The design allows for the use of both water and air medium trials. Using Air, a lung is attached to the top of the box as pictured above, effectively replicating the diaphragms control of the lungs in the human body. When testing with water, the box may be completely filled with water while still utilizing the simulated lung to separate water contaminated with flow visualization dye and volume control water. This design also allows for easy calibration of lung volume control through the use of a distance sensor detecting the pistons position and the known cross sectional area of the pistons face. With this design the lung may be isolated from any mechanical vibrations caused by the piston by connecting it to the box with a rubber hose. By using this rubber hose and clamping it down mid span we eliminate the chance of mechanical vibrations causing excessive noise in our pressure sensor signals as this had been an issue in previous attempts at constructing a similar device. The servomotor used is geared to drive the

piston's push-pull rack gear from both the top and bottom eliminating any friction in the piston that could be caused by an uneven driving force.

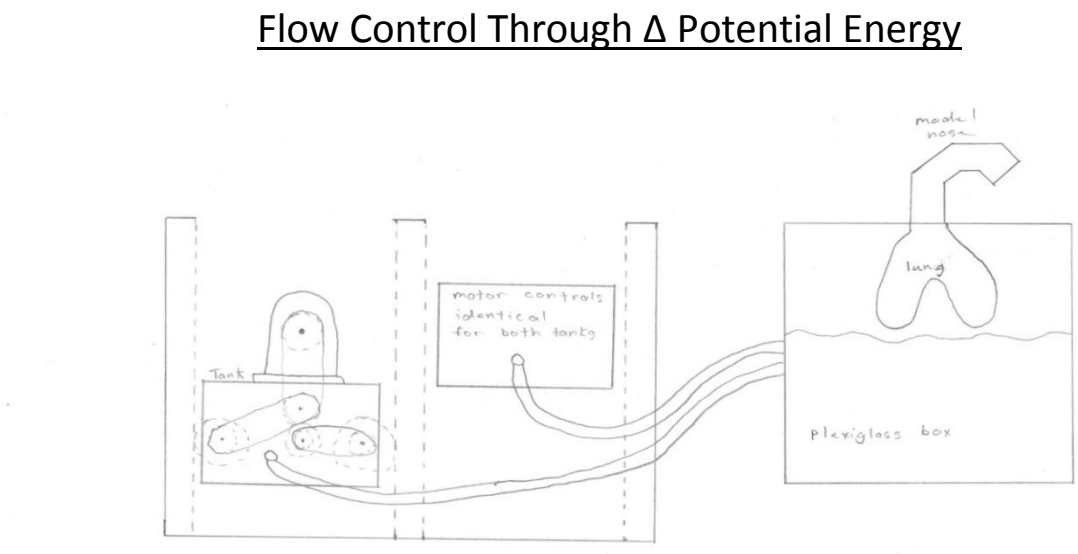

Figure 12: Flow control Through Change in Potential Energy

This design (Figure 12) utilizes the relation between change in height of our tanks and the rate at which water enters or exits the box. This design has all of the positive characteristics exhibited by other designs which isolated the lung from mechanical vibrations using the Plexiglas box. However, the design requires the control of two motors and to operate properly the size of the system would be very large and bulky. It also adds complexities to the flow rate calculations relating change in potential energy of the two tanks to the mass flow rate of water exiting and entering the Plexiglas box.

PRELIMINARY DESIGN MATRICIES

With several different design alternatives established, it is necessary to determine which design alternative best fulfills the previously determined weighted objectives. Therefore, a best of class chart was used to evaluate and rank the design alternatives in a semi quantitative fashion. For each objective, an increasing score was assigned to each design alternative. The scores

ranged from 1 to 4. A score of 1 for a design meant that it best fulfilled the compared objective, while a score of 4 meant the design did not fulfill the compared objective relative to the other designs. Ties were allowed when the design team felt that two or more designs fit the compared objective equally well. For example, when two design alternatives were considered best and were tied for first, the available rankings were added together and then divided by 2 to determine the assigned ranking for the tied designs. Table 5 shows the rankings for the best of class chart.

Best of Class Chart						
Design → **Objectives ↓**	Δ Potential Energy	The Pressurized Fish Tank	Linearly Controlled Piston With Isolated Lung	Pneumatic Piston Oscillator	Linearly Controlled Piston	Air Pressure Controlled Flow Rate
Low signal noise	5	2	1	6	4	3
Cost	6	2	4	1	3	5
Breathing flow rate accuracy	5	3	1	4	2	6
Accuracy	6	3	1	4	2	5
Visualization	5	1.5	1.5	4	3	6
Durability	5	4	2	3	1	6
User friendly	6	3	1	4	2	5

Table 5: Best of Class Chart (Without weighted objectives)

Once the conceptual designs were ranked in accordance to how well they fulfilled the design objectives, the previously determined objective weights were then applied. Table 6 shows the best of class chart incorporating the objective weights.

Best of Class Chart							
Design → **Objectives ↓**	*Weighted % ↓*	Δ Potential Energy	The Pressurized Fish Tank	Linearly Controlled Piston With Isolated Lung	Pneumatic Piston Oscillator	Linearly Controlled Piston	Air Pressure Controlled Flow Rate
Low signal noise	*.214*	1.070	0.428	0.214	1.284	0.856	0.642
Cost	*.095*	0.570	0.190	0.380	0.095	0.285	0.475
Breathing flow rate accuracy	*.286*	1.430	0.858	0.286	1.144	0.572	1.716
Accuracy	*.167*	1.002	0.501	0.167	0.668	0.334	0.835
Visualization	*.024*	0.120	0.036	0.036	0.096	0.072	0.144
Durability	*.119*	0.595	0.476	0.238	0.357	0.119	0.714
User friendly	*.080*	0.480	0.240	0.080	0.320	0.160	0.400
Total	*1*	*5.267*	*2.729*	*1.401*	*3.964*	*2.398*	*4.926*
Rank		**#6**	**#3**	**#1**	**#4**	**#2**	**#5**

Table 6: Best of class chart (incorporating weighted objectives)

For the best of class chart, the conceptual design with the lowest summed score was considered the best design alternative for the job. The isolated lung had the lowest summed score of 1.401 and was therefore considered the best design alternative. The runner up was the piston directly connected to the nose design with a score of 2.398. After analyzing the objectives and conceptual designs, the design team felt confident in choosing The Linear Controlled Piston with Model Lung as an initial design.

PRELIMINARY DESIGN

The initial design, section 4.2.2, consisted of a piston attached to a premade linear stage. The piston attached to the stage's positioning plate and the cylinder was mounted to the positioning plate's guide. An example of a prefabricated linear stage can be seen in figure 13.

Figure 133: Prefabricated Linear Stage

The linear stage allowed the team to align the piston and cylinder and have precision control of the piston position. However, there was a serious flaw with this design: because the team would be mounting the piston assembly to the stages' positioning plate, the force caused by the piston would create a moment on the guides of the stages' positioning plate. This problem eliminated any cheaper linear stages which utilized a friction slide joint. Other linear stages were too expensive due to their extreme precision which was not a requirement of this project. Therefore, the team then decided to design and construct our own linear stage subject to our specifications.

The stage would have to be lightweight and small enough to be easily carried by a single person. The piston's cross sectional area and travel distance determined the size of the device. These calculations will follow in the Piston Requirements section 4.4.2.

The Piston Assembly

The main components of the piston assembly consist of the piston, cart, guide rods and brackets as seen in Figure 14. The piston assembly acts as the diaphragm in the human body. The motor is attached to the cart by a ball screw rod that moves the piston to push the proper volume of medium to a Plexiglas box where the model nasal cavity is attached. The motor is controlled to move at an unsteady state to replicate the proper breathing curve.

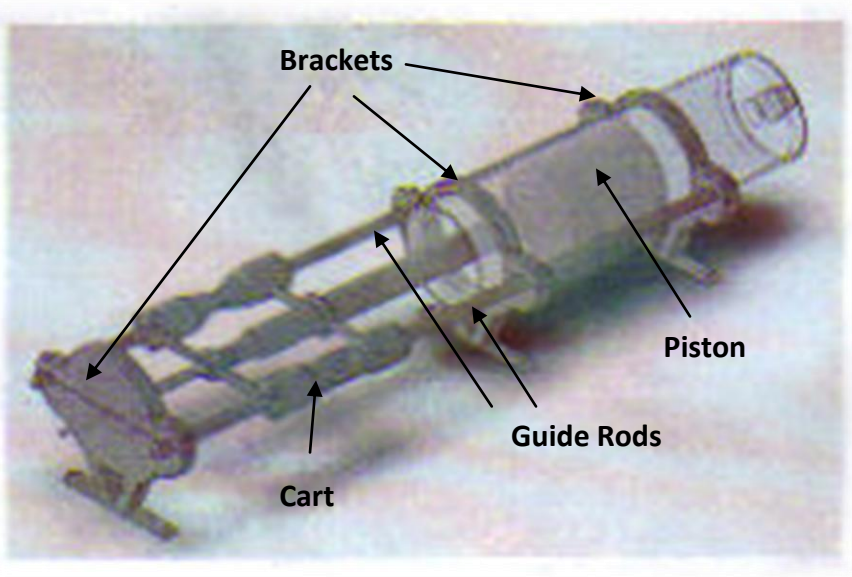

Figure 14: The Piston Assembly

Piston Requirements

First, the team had to determine the diameter, length and tolerance of the piston before designing the cart and brackets, and length of the guide rods.

Diameter of Piston

To determine the size of the piston, the design team analyzed the travel distance required to achieve our maximum lung volume, 1.3 liters. From the graph in Figure 3, the maximum tidal volume is about .65 liters. However, since the model nasal cavity is twice the size of a human, the tidal volume needed to be doubled to account for this scaling.

The readily available piping sizes varied between 1 and 8 inches for the outside diameter of the tubing that enclosed the piston. All the tubing had a wall thickness of .125 inches. By using the equation for volume,

$V = Length * Cross\ sectional\ Area$, the distance the cart would travel was calculated. These data are shown in Table 7.

Determining the Outer Diameter of the Cylinder		
$1.2\ Liters = 73.2\ cubic\ inches$		
Outer Diameter of Pipe [inches]	**Cross Sectional Area [inches]**	**Length of Travel [inches]**
8	47.2	1.5
6	26.0	2.8
5	17.7	4.1
4	11.0	6.6
3	5.9	12.3
2	2.4	30.5
1	0.4	165.8

Table 7: Determining the Outer Diameter of the Cylinder

From analyzing the table, the design team eliminated eight and six inch tubing because the distance of travel was too small to achieve accurate resolution and eliminated the one to three inch diameters because the travel would be too long. This left the team to choose between 4 and 5 inch pipe. The 4 inch pipe was chosen for the smaller diameter of the piston and accuracy due to its larger travel.

Length of the Piston

The length of the piston was originally determined to be 6 inches, making our piston length > 1.5 * piston diameter. This is to ensure correct tracking of the piston inside the cylinder so that it cannot bind during travel. For weight reduction the piston will be hollowed out as much as possible with considerations for strength and our machining capabilities. This reduces

the inertia and kinetic energy of the moving parts of the piston assembly. A SolidWorks drawing of the preliminary piston design can be seen below in Figure …

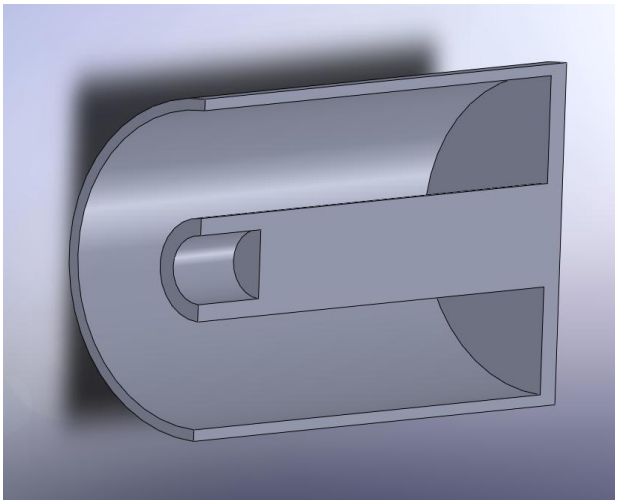

Figure 14

Tolerance

After determining the cylinder size, the design team had to determine the tolerance of the cylinder. A six foot length of transparent plastic tubing was purchased for the cylinder. The inside diameter of the piston cylinder was given by the manufacturer to be 3.75 ± .03 inches. To accommodate this, the outside diameter of the piston was turned to 3.72 inches to allow for proper clearance between the pistons hard surface and the inside of the plastic cylinder. To determine the best inside diameter a series of O ring test grooves were then turned into the side. The purchased O rings were coated with a cooking oil lubricant and then test fitted on each groove. The seal of the O ring was tested using a hydraulic test as shown in Figure 15. Through this method, the proper inner diameter of the O ring was found to be 3.36 inches.

Figure 15: Test Method for O Ring

Cart

The cart functions to transform the circular motion of the motor to the linear motion of the piston. To ensure tracking on the guide rods which align the piston assembly, four linear bearings were positioned at the four corners of the cart. The length of the cart had to be taken into account in the minimum overall length of the guide rods. Clearance through the middle of the cart, with the bearings passing along the outside of the cylinder was necessary to reduce the overall length of the assembly. This allowed for shorter guide rods and decreased cost.

The third and most important design factor was the ability to manufacture all parts in a reasonable amount of time. A chronological progression of the cart design is shown in Figure 16. These designs were unfeasible due to a lack of available tools, functionality of the machines, and lengthy machining time. The first two iterations were too difficult to manufacture because the CNC milling machines operate along orthogonal axes, making the interior curves impossible to create with the given technology. The third design shown in Figure 16 was too cumbersome to machine because of its intricate curves and multiple pieces. Completion of these carts would

take too much time, so the cart was redesigned around the capabilities of the available machines and tools.

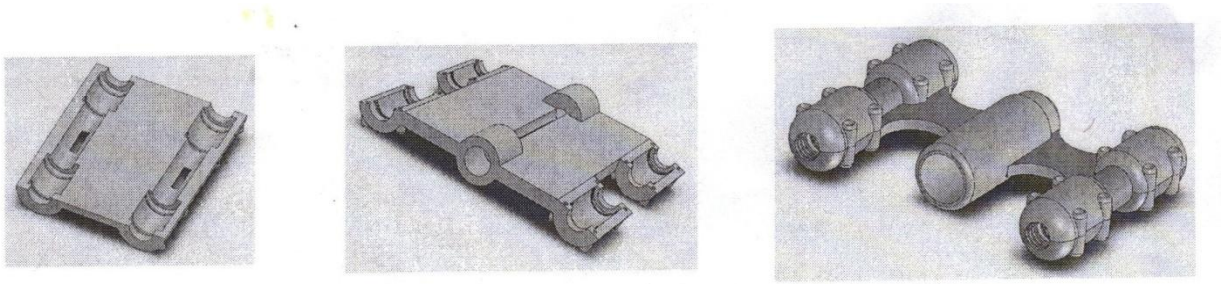

Figure 16: Preliminary Cart Iterations

Guide Rods

The guide rods were chosen to be precision ground chrome plated steel. The chrome plating is to prevent corrosion since we will be using water. Normal ½ inch rods have a diameter measuring approximately .50 ± .02 while a precision ground rod will have a diameter of .500 -.001. The specified linear bearings are designed to work on rods of diameter less than or equal to the specified inner diameter, so rods in excess of this diameter would not allow the bearings to travel. Also, the guide rods had to be thick enough to support and align the entire piston assembly without warping or deformation due to the internal working forces of the machine. As the diameter of the piston increases, the size and costs of all other components also increases because they need to be more robust. After weighing the cost of the rods against their resiliency, ½ inch rods with a length of 36 inches were chosen and would meet all of the requirements at a reasonable price.

Brackets

All the parts of the piston assembly are connected together with brackets designed with Solidworks. Two of the three brackets have a large central opening, while the third does not (Figure 14). The brackets hold the guide rods on which the cart travels, providing rigidity and keeping them parallel and in line with the piston cylinder. The two similar brackets, shown in Figure 17, hold the piston cylinder equidistant between the rods, with all three central axes held in the same plane. The third bracket holds the beginning of the ball screw, keeping it in plane with the rods and the piston cylinder.

Figure 17: The Two Similar Brackets

The Tank and Delivery Tube

The piston assembly is attached to a flexible delivery tube that connects the end of the piston cylinder to the tank. The clear Plexiglas tank was based on that of the previous project, and modified to be a closed unit with a rubber pipe fitting at the top and bottom. The model nasal cavity was attached to the pipe fitting on the top of the tank allowing it to breath with the desired flow rate produced by the piston assembly. The tank acts as the lungs in the human

body. When breathing air, the tank is filled half full with water, forcing air in and out of the nose. When breathing water, the tank is filled to the top with water so that the water in the tank is also forced in and out through the nose. The delivery tube was attached through an opening at the bottom of the tank through a 1.5 inch PVC pipe. When experiments are complete, water is removed through a half inch interior diameter tube connected through the bottom of the tank.

Motor and Controls

The motor will be a brushless dc stepper motor controlled with a closed loop system using a linear potentiometer for feedback. The actual control will be done through computer software and the motor will be connected to a Newport industries esp300 motor controller which is available for use from the school. The size of the motor will be finalized upon completion of the piston assembly construction.

4.5 Final Design

Though the final initial design excelled in many areas, the team found that components would not function properly without having to be redesigned. Our motor would have to spin up to a few thousand rpm, stop and change direction all in a matter of seconds to mimic the unsteady breathing curve. A motor control that requires this large speed changes in a short amount of time, while still being accurate, is expensive and not within budget constraints of the project. Therefore, the piston assembly was redesigned to include a mechanical linkage to connect the motor to the cart. This linkage transformed the rotational motion of the motor into a sinusoidal linear motion of the piston. The final design is pictured in Figure 18 with the preliminary design and the changes discussed in detail.

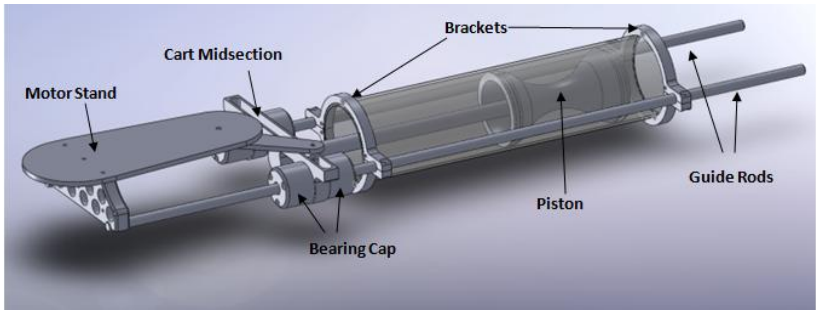

Figure 158: Labeled Piston Assembly-Final Design

Figure 19: Preliminary Piston Assembly

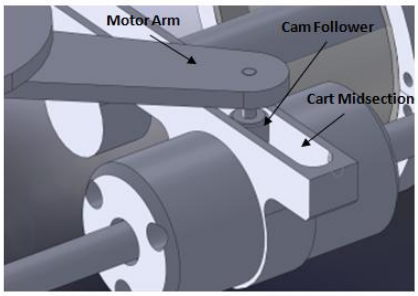

Figure 160: Detailed View of Cart Midsection

Drive Mechanism

The most important and noticeable change is the complete redesign of the drive mechanism. Our final preliminary design used a high speed motor and a quadrature encoder to position the cart using a ball screw and nut. The final design utilized a slow speed servomotor and a linear potentiometer to position the cart with a scotch yoke mechanism. This was much easier to control as it did not require spinning up to a high speed, stopping and changing direction in a short period of time.

Cart

To adapt to the new control method, the cart had to be redesigned. Aided with the knowledge of the schools available CNC tooling, the cart was redesigned with ease of manufacturing in mind. Previous cart iterations were composed of up to nine individual pieces, a

total of five different part drawings. The final cart design, Figure 21, had only five pieces and two part drawings. This greatly reduced both the coding and the machine times. The cart midsection was redesigned with a track for a cam follower to slide, a configuration known as a scotch yoke. It also had tapped holes to screw the four bearing caps to. The two faces that the bearing caps would be attached to were machined flat and parallel to each other, insuring that the bearings would be aligned.

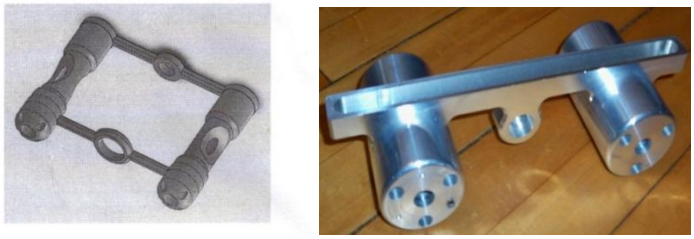

Figure 171: Preliminary Cart Design Versus Final Cart Design

Piston

The preliminary piston design had the shape of a coffee can with a lid with the bottom acting as the face of the piston (Figure from 4.4). This design was not feasible to machine due to the available tools. The available lathe tool did not have a deep enough reach to machine the interior. The design was changed to resemble an hourglass. The new piston was designed with the ease of turning and weight reduction in mind. The length remained the same as in the preliminary final design and the O ring diameter was determined in the manner described in the preliminary design section.

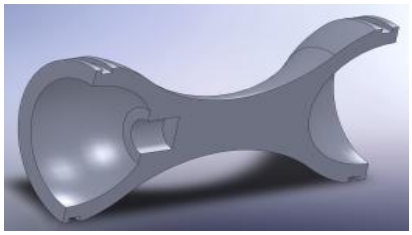

Figure 22: Cross Sectional View of Final Piston Design

Rods

After the assembly was designed, the team chose three foot steel rods to prevent any spacing issues of the components in the piston assembly. Thirty six inch rods would provide sufficient space for all components to function as intended.

Brackets

The preliminary brackets had already been machined when the piston assembly was redesigned. It was decided that the next brackets did not need to have stands. The guide rods are strong and sturdy enough to support the brackets without them having to be bolted to the ground. A wooden stand equipped with rubber feet to lessen vibrations held the ends of the rods holding the assembly aloft.

4.6 Motor and Control

Once the piston assembly was constructed, it was very crucial to focus on the motor and how to control the machine through computer software. The goal of the machine was to control tidal volumes and respiration rates so anyone can analyze various unsteady state nasal flow patterns. To accomplish this goal, the proper motor and controls were necessary so that the machine could accurately simulate human breathing.

The control system consisted of a Vex microcontroller, a signal processor, and string linear potentiometer. The team decided on a closed loop system utilizing the string potentiometer feedback to provide us with the most accurate and easily adaptable control method. Our program focused on making the machine breath exactly as one individual did, but

have the capability to easily change the prescribed breath volume and flow rate with respect to time.

The sample breath taken from the recorded lung volumes in figure 3 was digitized into 20 different points with the program Bytescout Graph Digitizer giving us an excel table containing lung volumes taken at even time intervals as shown below in figure … The maximum lung volume was then determined and all values were divided by it giving us a percentage of overall lung volume at all 20 of the digitized points taken from the graph.

By design the scotch yoke mechanism allowed one breath including inhalation and exhalation without stopping the motor or changing its direction. The pure sinusoidal linear motion produced by a constant motor speed scotch yoke is very close to the natural breathing rhythm of a human. To change the lung volume while still maintaining one revolution per breath the scotch yokes effective arm length may be changed affecting the total volume of air moved in one breath.

For our sample breath the effective arm length was set to 3.57 inches giving us a lung volume or 1.3 liters. The minimum and maximum linear potentiometer readings which correlated to the two positions where the yokes arm was parallel to the guide rods were observed through the Easy C On-Line build window and recorded. This range of values was then multiplied by the percentage of total lung volume for each of the 20 points giving us a linear potentiometer reading for each of the desired positions. These values were then tabulated and accessed by the vEx microcontroller as desired targets which changed every 40 milliseconds giving us a four second breath with a desired string potentiometer setting for that time. The motor was then instructed to adjust its speed based on the multiplier of the difference between its current string potentiometer

reading and the desired position at that time. The schematic of our system may be seen below in figure …

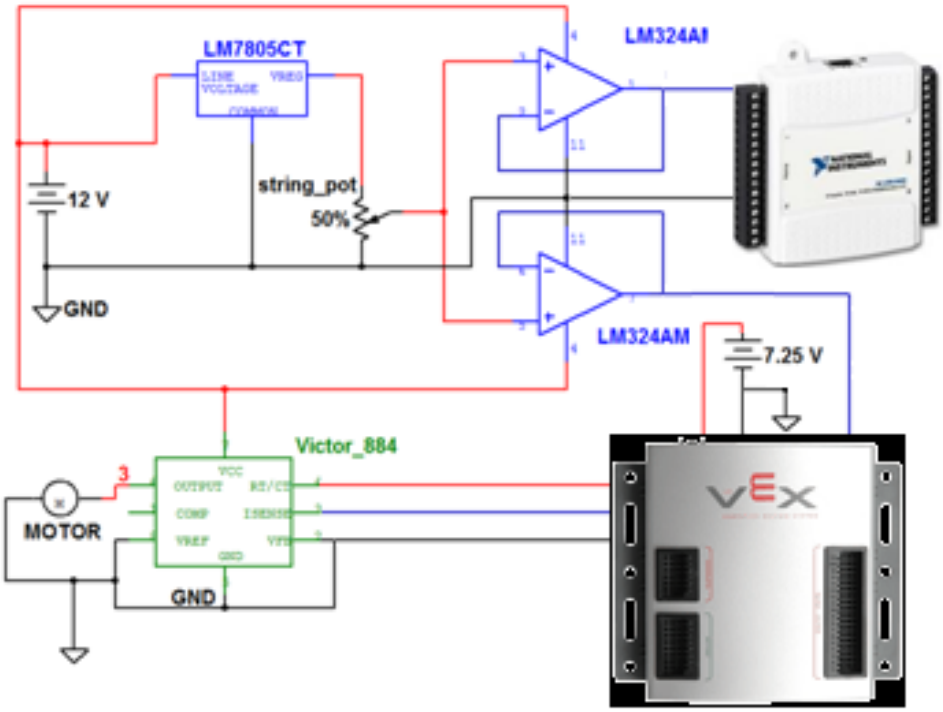

Final Design Modification

Once the device was constructed, a few adjustments needed to be made in order for it to work properly. The two main components that needed to be focused on were the cart and the piston. Both components needed to be redesigned in order for the device to achieve the proper flow rate to replicate the human breathing curve.

Cart

When the device was on, the cam follower would bind up in the cart's midsection. This did not allow the device to run smoothly and needed to be redesigned. To prevent this from occurring, the cam follower was completely eliminated. Two small plates were made that fitted

on each end of the cart's midsection to allow two parallel guide rails to run through. Instead of a cam follower, two self aligning sealed linear bearings were purchased to slide on the guide rails. This prevented any binding and allowed for smooth rotation of the scotch yoke mechanism. The modified cart is shown in Figure # with the piston.

Piston

The piston needed to be designed because the O rings were designed for a stationary fit and we had a dynamic use. The new piston design was composed of two plates which bolted together and held the O ring in its original unstretched size. This allowed the least amount of friction while providing a seal. With this new design, the O ring was not compressed against the cylinder wall. As the piston moved, the friction between the O ring and the cylinder wall slightly pulled the O ring out of its groove providing the desired airtight seal.

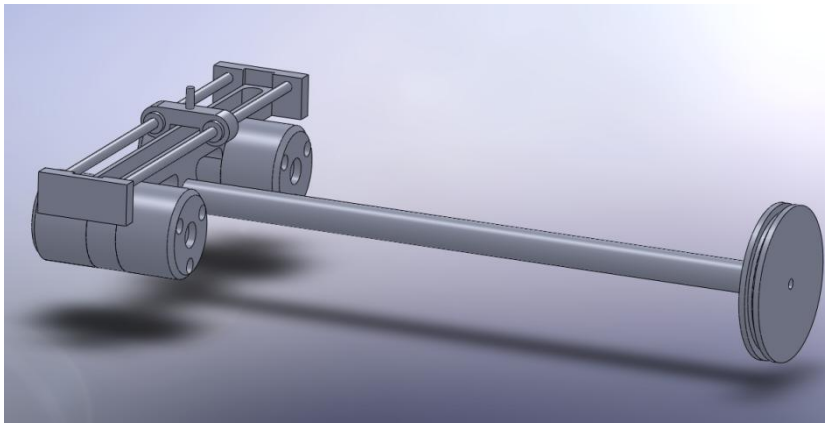

Final Assembly

The entire assembly, including all of the components, could be seen in Figure #. PVC tubing caps were used to attach the flexible vinyl tube to the end of the cylinder. The 1.5" OD clear flexible tubing attached the piston assembly to the box and was secured tightly with clamp.

Chapter 5: Methodology

This chapter will thoroughly discuss the virtual instrument in LabView and the methods for data collection used during the experiment.

Breathing Curve

From the Handbook of Physiology: Respiration [11], the volume versus time and pressure versus time graphs (Fig 3) were obtained for the human breathing curve. These two curves were placed into the Byte Scout Graph Digitizer software program. This program automatically converted these two hard copy graphs into X and Y coordinates, which could easily be exported to Excel. Therefore, proper motor control could be obtained by replicating the curves from their coordinate system.

Scaling

Since the model nasal cavity is twice the size of a human nasal cavity and the device breathes both water and air, proper scaling was required for the device to simulate normal breathing flow rates. Through analysis using the Reynolds number (eq. #), Womersley number (eq. #), and Euler's constant, the volumetric flow rate, pressure differential, and breathing frequency were scaled respectively. For a more in-depth analysis of these equations, see Appendix A.

	2x Water Model	2x Air Model
Flow Rate, $\dot{Q}_m(t)$	$0.129\dot{Q}_{nose}(t)$	$2\dot{Q}_{nose}(t)$
Breathing Frequency, ω_m	$1.615 \times 10^{-2}\ \omega_{nose}$	$\frac{1}{4}\omega_{nose}$
Fluid Pressure, P_m	$0.8722P_{nose}$	$\frac{1}{4}P_{nose}$

Programming the Motor

The 12 volt DC motor was controlled by a vEx brand microcontroller used in conjunction with EasyC software and a Victor 884, 12 volt motor speed controller. The extrapolated data points in Excel were graphed into pressure versus time and volume versus time graphs to act as the control data. The originally planned closed loop motor control would not function properly due to an undersized motor. Due to budget constraints the team chose a free motor available for use from the schools robotics department. Since the natural sinusoidal linear motion produced by the scotch yoke mechanism closely matches the desired breathing curve (Fig #), it was determined that a single motor speed could initially be set for the entire breath and then adapted to more closely match our desired curve. The C code and Easy C screen are shown in appendix XXX.

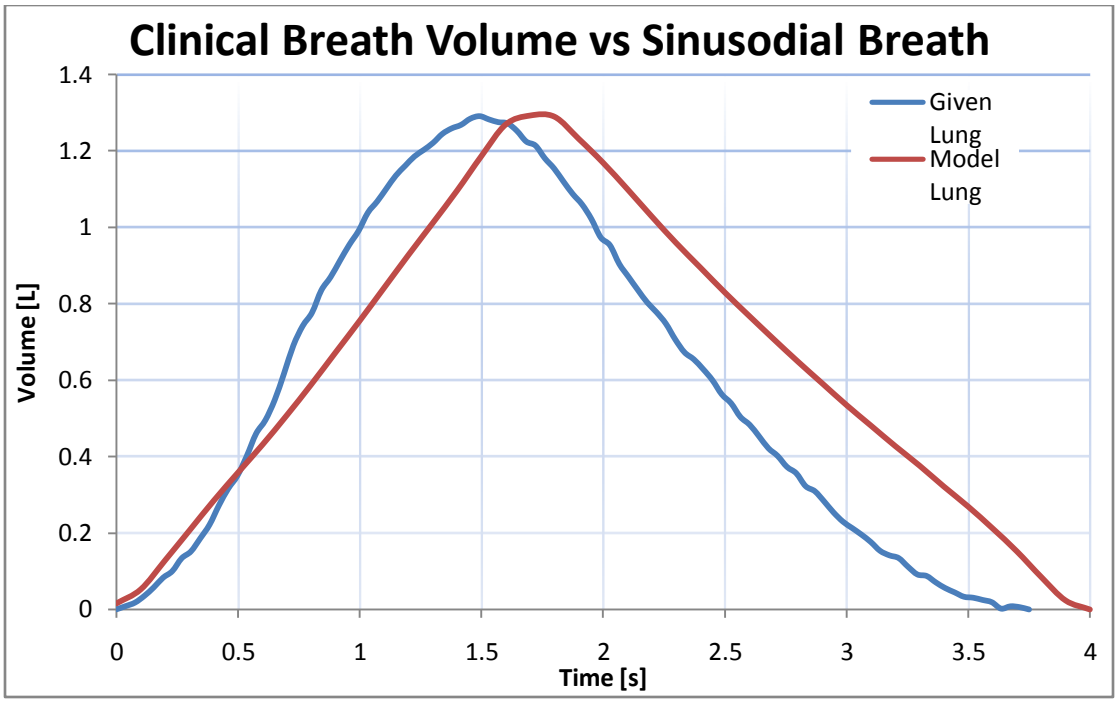

The breath was divided into twenty 20 millisecond periods with an individual motor speed set for each period. The data produced by the device was then plotted versus the control data, and the speed was increased or decreased by sections according to how well it matched the control data, until the closest fit possible. These values are heavily influenced by the amount of friction inside of the piston, and needed to be reset for each build of the device. The final volume output can be seen graphed against the given lung volume in figure $.

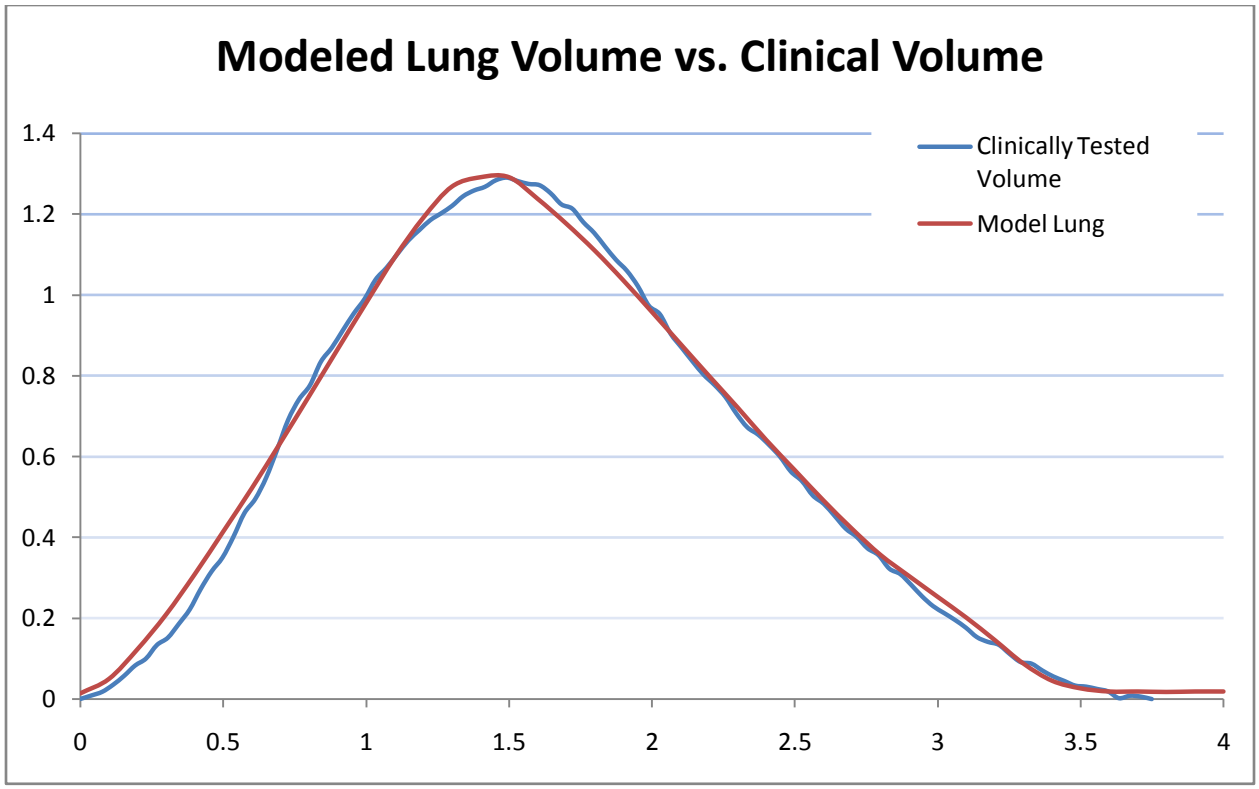

Data Collection

To measure the pressure, a low differential pressure sensor was purchased from Sensiron. Sensor model? This sensor was chosen after predicting the approximate pressure readings that were to be expected from previous scaling using the Euler's Constant (see Appendix A). After scaling, it was determined that the pressure in the model nasal cavity should be four times the pressure in a human nasal cavity.

The differential pressure sensor was attached to a 4 mm ID clear flexible tubing located at the tip of the nose and just below the nasal model in the rubber pipe fitting. The sensor was wired to a National Instrument USB DAQ 6008 allowing us to collect and analyze the voltage signal output by our pressure sensor.

Our data collection also needed to include the position of the cart allowing us to calculate lung volume and insure the accuracy of each breath during data collection. To allow for the collection of the string potentiometers signal from both the vEx microcontroller and the USB

DAQ the signal was conditioned using a simple operational amplifier circuit shown in Figure # the wiring diagram wherever it is.

The LabView virtual instrument (VI) needed to be constructed to display the pressure and the position of the piston, as well as write the data to files for Excel so they could easily be analyzed. Both of our sensors gave a differential voltage output which was easily converted to the values we wanted using LabView. The pressure sensor data was converted to cm of H_2O by importing a table of the sensor~~s~~ pressure readings and the~~re~~ corresponding voltages **APPENDIX**. The string potentiometer's voltage output scaled linearly so only a maximum and minimum voltage and lung volume were provided to automatically scale to Liters of air. With this VI, when opening the files in Excel, three columns of data are produced: time, pressure, and lung volume. The Front Panel and Block Diagram for this virtual instrument were as seen in figure #.

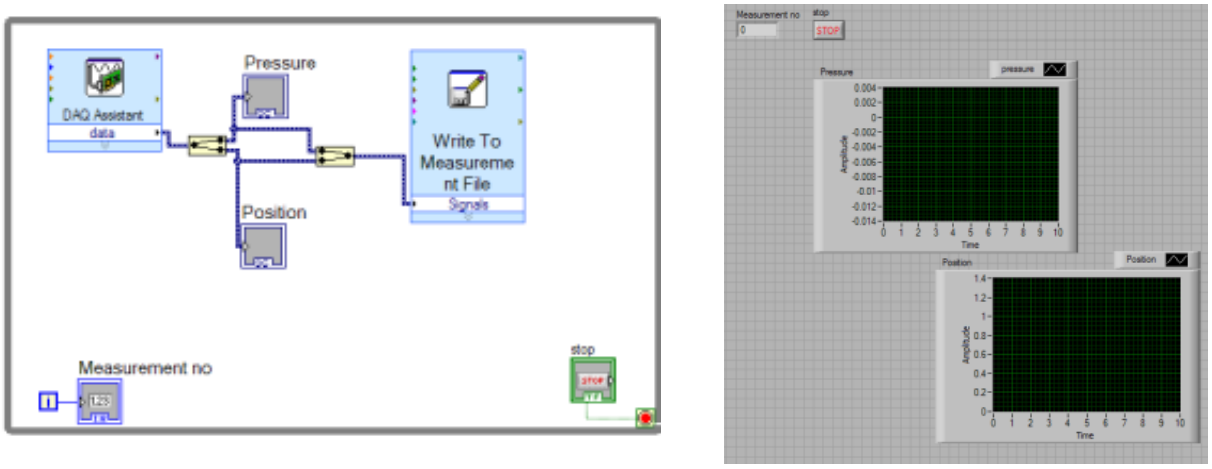

Figure 18#: Front panel of the Virtual Instrument

Testing

Ten trials for each model nasal cavity were taken following the procedure in Appendix # and the pressure and volume data were recorded. Since the modeled nasal cavities were given to the team from a previous group, the team was unsure which model was pre-surgery and which was post-surgery. The analysis allowed a determination to be made.

Chapter 6: Results

Our device was able to mimic the human breathing flow rate. Also, the pressure drops across the nasal cavity in the pre- and post-surgery models were recorded and were quantitatively compared.

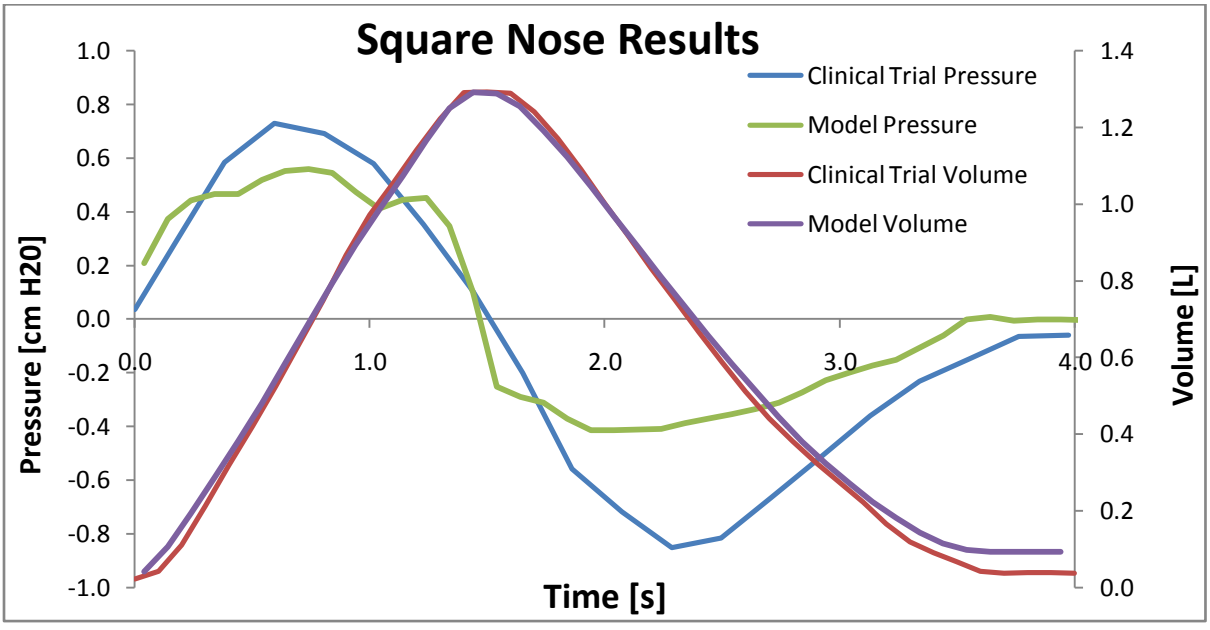

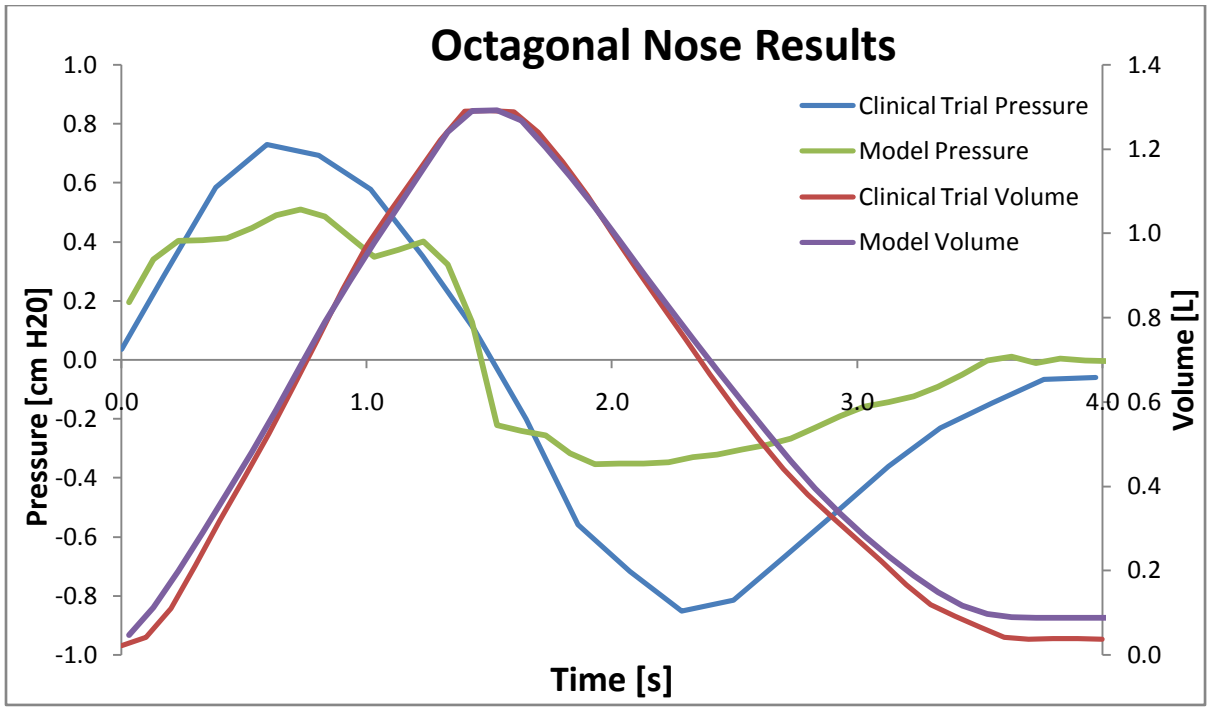

FLOW MEASUREMENTS

The average of flows obtained from the device pre-and post- surgery are shown in Figure #. This figure combines the data averaged for ten trials for each condition and compares it against the clinical volume.

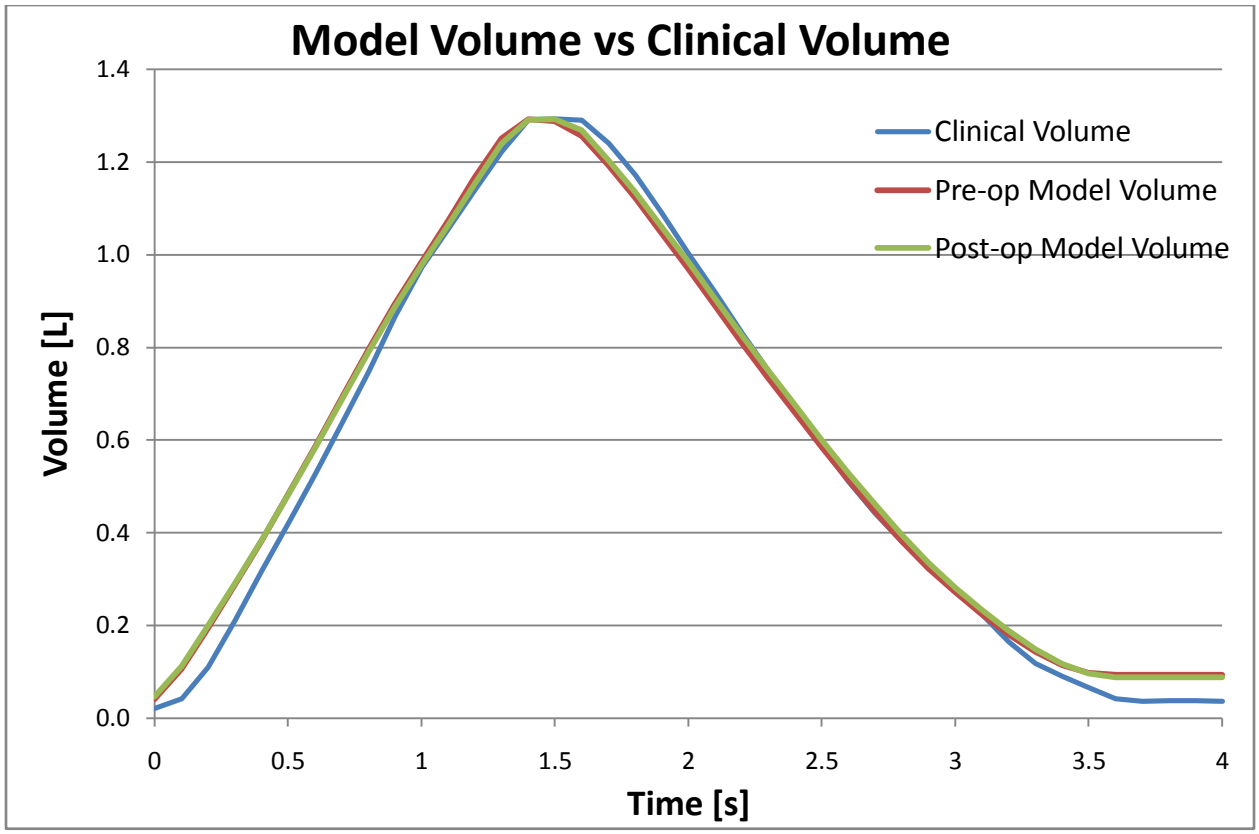

PRESSURE DATA

The recorded pressure vs. time for the normal and post turbinectomy models is shown in figure.. Once again, this figure is an average of ten pressure trials for both pre-and post operation models and is compared against the clinical pressure.

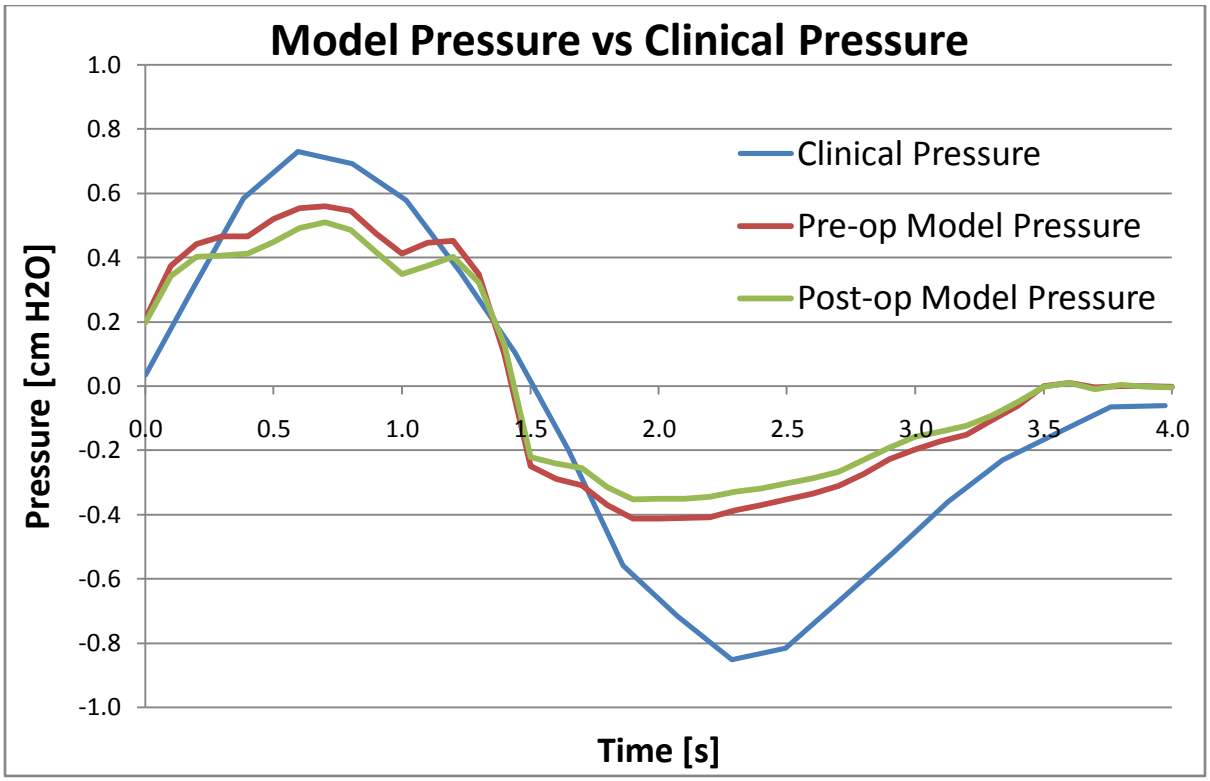

Chapter 6: Conclusions

Appendix A: Scale Flow Calculations

The true nose breathes a volume $Q(t)$ $[cm^3]$ each breath at a rate of $\dot{Q}(t)$ $[cm^3/s]$. To accurately equate this to the give double scale model, the Reynolds Number must be employed.

$$Re = \frac{4\dot{Q}(t)}{\pi d \nu}$$

To equate the real nose, denoted by n, to the model that breathes air, denoted by $m\ air$, and water, denoted by $m\ water$, the two equations for the common Reynolds Number are equated;

$$\frac{4\dot{Q}_n(t)}{\pi d_n \nu_{air}} = \frac{4\dot{Q}_m(t)}{\pi d_m \nu_m} \quad \textbf{(1)}$$

The kinetic viscosity, ν, for air and water at 70°F were given to be

$$\nu_{air} = 1.521 \times 10^{-5}\ m^2/s,$$

$$\nu_{water} = 9.817 \times 10^{-7}\ m^2/s.$$

The scaled flow rate for the **double scale air breathing model** was calculated to be:

$$\frac{4\dot{Q}_n(t)}{\pi d_n \nu_{air}} = \frac{4\dot{Q}_{m\ air}(t)}{\pi 2 d_n \nu_{air}}$$

$$2\dot{Q}_n(t) = \dot{Q}_{m\ air}(t) = A_{x-sec} \cdot V_{air}(t). \quad \textbf{(2)}$$

The scaled flow rate for the **double scale water breathing model** was calculated to be:

$$\frac{4\dot{Q}_n(t)}{\pi d_n \nu_{air}} = \frac{4\dot{Q}_{m\ water}(t)}{\pi 2 d_n \nu_{water}}$$

$$\left(\frac{2 \cdot \nu_{water}}{\nu_{air}}\right)\dot{Q}_n(t) = \dot{Q}_{m\ water}(t)$$

$$0.129\dot{Q}_n(t) = \dot{Q}_{m\ water}(t) = A_{x-sec} \cdot V_{water}(t). \quad (3)$$

The cross sectional area of the piston chamber, A_{x-sec}, must remain a constant throughout the experiments. To switch between breathing air and breathing water the piston velocity must absorb the difference in flow rates. The ratio of these velocities was calculated by solving equation (2~~(2~~) for the cross sectional area and substituting into equation (4~~(4~~):

$$15.48 = \frac{V_{air}(t)}{V_{water}(t)} \quad (4)$$

The frequency of breathing was also affected by the change in scale and medium. To correct for this change the Womersley Number was used to scale the breathing frequency.

$$\alpha = R * \sqrt{\frac{\omega}{v}}$$

To equate the real nose to the model that breathes air and water, the two equations for the common Womersley Number are equated;

$$R_n \cdot \sqrt{\frac{\omega_n}{v_{air}}} = R_m \cdot \sqrt{\frac{\omega_m}{v_m}} \quad (5)$$

The scaled breathing frequency for the **double scale air breathing model** was calculated to be:

$$R_n \cdot \sqrt{\frac{\omega_n}{v_{air}}} = 2R_n \cdot \sqrt{\frac{\omega_{m\ air}}{v_{air}}}$$

$$\frac{1}{4}\omega_n = \omega_{m\ air} \quad (6)$$

The scaled breathing frequency for the **double scale water breathing model** was calculated to be:

$$R_n \cdot \sqrt{\frac{\omega_n}{v_{air}}} = 2R_n \cdot \sqrt{\frac{\omega_{m\ water}}{v_{water}}}$$

$$\frac{v_{water}}{4v_{air}} \cdot \omega_n = \omega_{m\ water}$$

$$1.615 \times 10^{-2}\ \omega_n = \omega_{m\ water} \quad (7)$$

To switch between breathing air and water, both frequencies will need to be compatible with the motor. To better understand the difference in frequencies, their ratio was calculated by substituting equation (6) into equation (7):

$$15.48 = \frac{\omega_{m\ air}}{\omega_{m\ water}} \tag{8}$$

It was found in equations (2) and (3) that the product of the cross sectional area and the instantaneous velocity was a constant with a time dependence. The range of flow rates in the human nose through one breathing cycle was then found to create an expression relating the cross sectional area to the instantaneous velocity.

$$\dot{Q}_{n\ max} \approx 0.4\ L/s\ = 400\ cm^3/s$$

$$\dot{Q}_{n\ min} \approx -0.5\frac{L}{s} = -500\ cm^3/s$$

Through unit analysis it was determined that $\dot{V}$ had units of cm/s and A_{x-sec} had units of cm^2. The minimum and maximum velocities of the **double scale air breathing model** were calculated using equation (2) to be:

$$\dot{V}_{m\ air\ max} \cdot A_{x-sec} \approx 200\ cm^3/s$$

$$\dot{V}_{m\ air\ min} \cdot A_{x-sec} \approx -250\ cm^3/s \tag{9}$$

The minimum and maximum velocities of the **double scale water breathing model** were calculated using equation (3) to be:

$$\dot{V}_{m\ water\ max} \cdot A_{x-sec} \approx 51.6\ cm^3/s$$

$$\dot{V}_{m\ water\ min} \cdot A_{x-sec} \approx -64.5\ cm^3/s \tag{10}$$

The third parameter of interest is the fluid pressure at various points in the flow. The pressure in a real nose can be equated to our model through the use of Euler's Constant:

$$E_u = \frac{P}{\rho \times V^2}$$

$$V_{nose} = \frac{\dot{Q}_n}{A_n}, \qquad V_{model} = \frac{\dot{Q}_m}{A_m}$$

In this equation, P is pressure, ρ is fluid density and V is the fluid velocity. The density of air and water at 70°F were given to be

$$\rho_{air} = 1.1934\ kg/m^3,$$

$$\rho_{water} = 997.97\ kg/m^3.$$

The constant must be the same through all models, so the standard set by the human nose can be equated to the double scale model

$$\frac{P_{nose}}{\rho_{air} \times \left(\frac{\dot{Q}_n}{A_n}\right)^2} = \frac{P_{model\ fluid}}{\rho_{model\ fluid} \times \left(\frac{\dot{Q}_{model}}{4A_n}\right)^2}. \quad (11)$$

When the model is breathing air, equations 2 and 11 reveal

$$\frac{P_{nose}}{\rho_{air} \times \left(\frac{\dot{Q}_n}{A_n}\right)^2} = \frac{P_{m\ air}}{\rho_{air} \times \left(\frac{2\dot{Q}_n}{4A_n}\right)^2}$$

$$\frac{1}{4}P_{nose} = P_{m\ air} \quad (12)$$

When the model is breathing water, equations 3 and 11 reveal

$$\frac{P_{air}}{\rho_{air} \times \left(\frac{\dot{Q}_n}{A_n}\right)^2} = \frac{P_{water}}{\rho_{water} \times \left(\frac{0.12917\dot{Q}_n}{4A_n}\right)^2}$$

$$0.8722P_{nose} = P_{m\ water} \quad (13)$$

The key equations used in relating the real nose to the double scale model are

	2x Water Model	2x Air Model
Flow Rate, $\dot{Q}_m(t)$	$0.129\dot{Q}_{nose}(t)$	$2\dot{Q}_{nose}(t)$
Breathing Frequency, ω_m	$1.615 \times 10^{-2}\ \omega_{nose}$	$\frac{1}{4}\omega_{nose}$
Fluid Pressure, P_m	$0.8722P_{nose}$	$\frac{1}{4}P_{nose}$

Appendix B

Large Linear Bearings

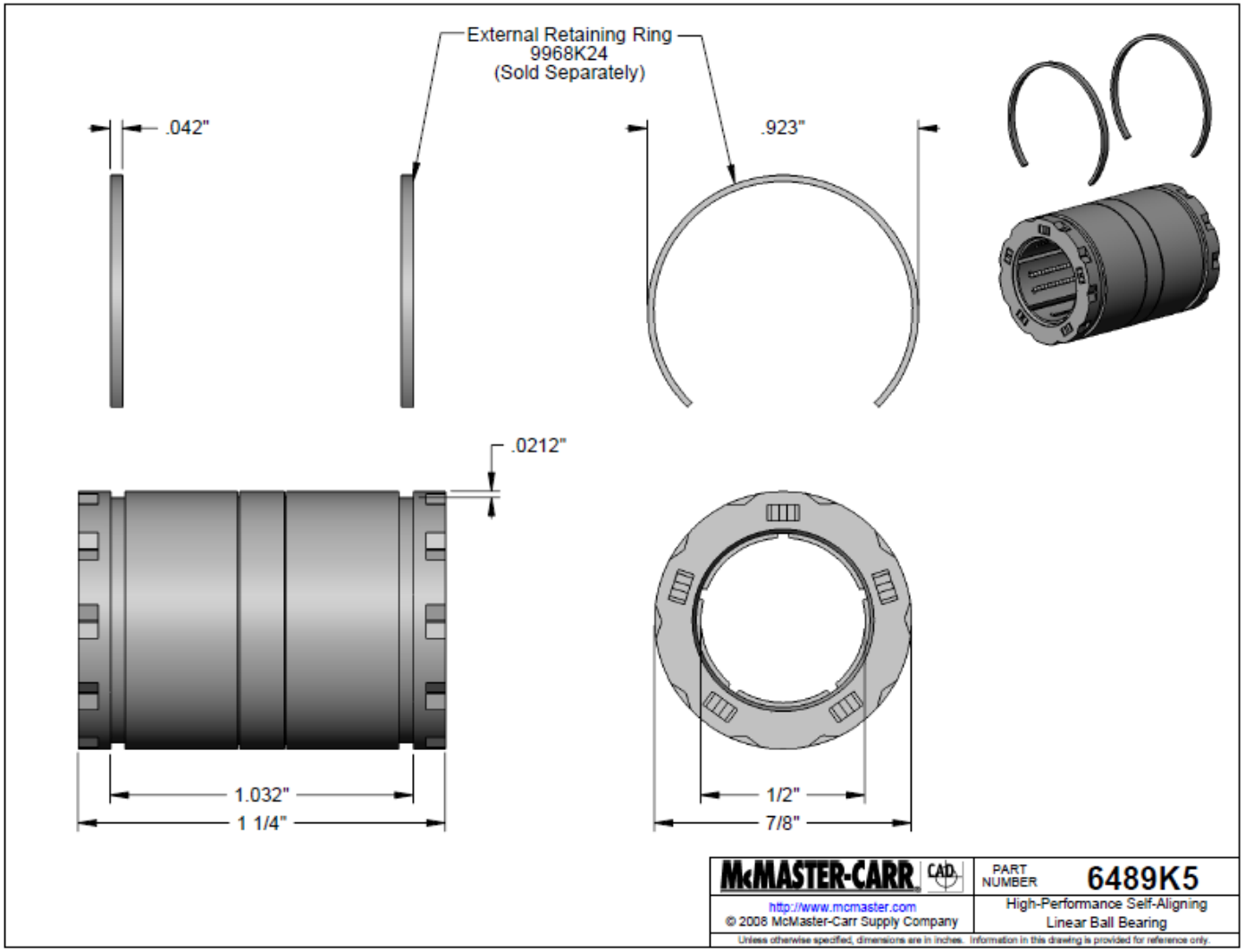

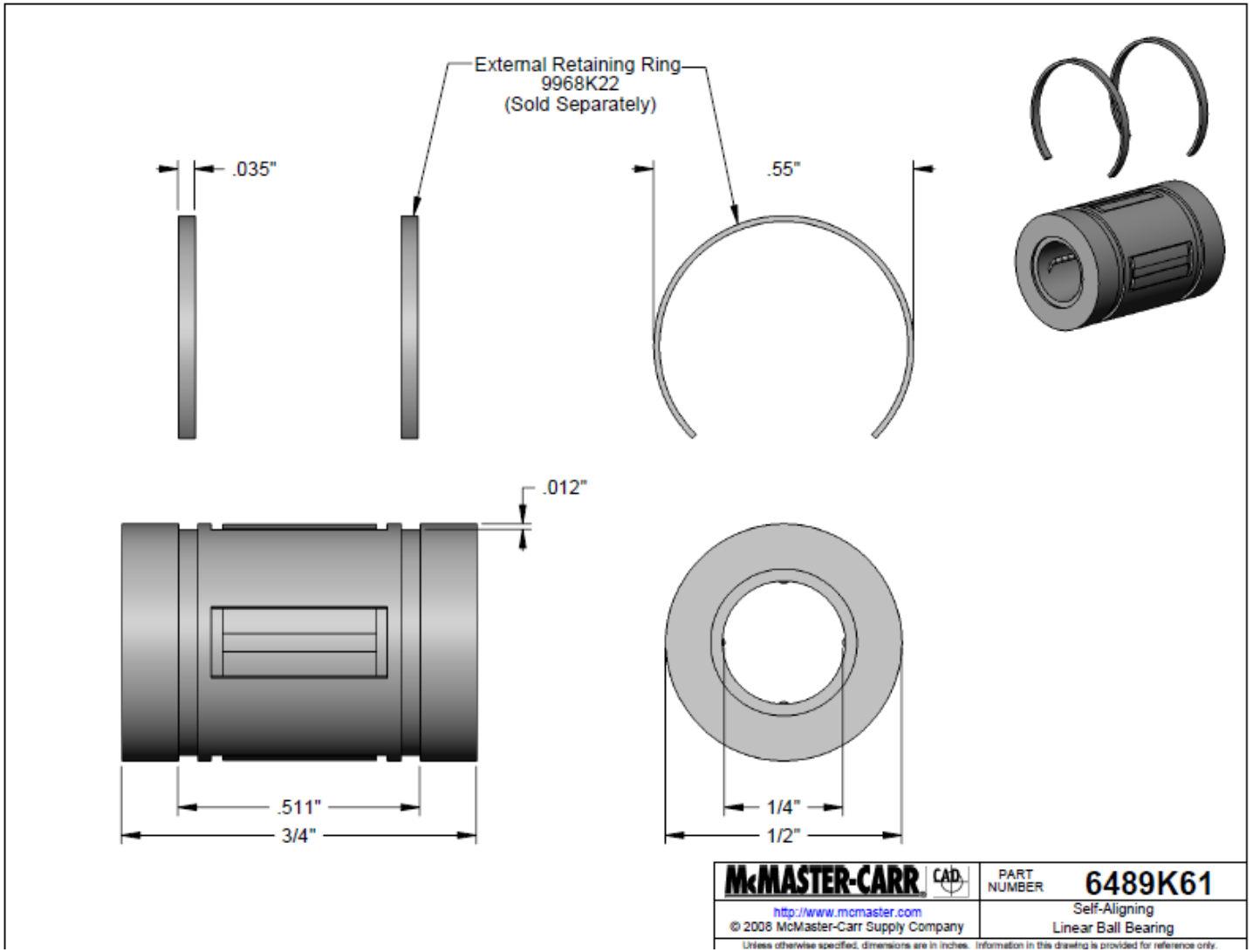
External Retaining Ring
9968K22
(Sold Separately)
.035"
.55"
.012"
.511"
3/4"
1/4"
1/2"
McMASTER-CARR
CAD
PART NUMBER
6489K61
http://www.mcmaster.com
© 2008 McMaster-Carr Supply Company
Self-Aligning
Linear Ball Bearing
Unless otherwise specified, dimensions are in inches. Information in this drawing is provided for reference only.

Precision Shafts

This product matches all of your selections.

Part Number: 6061K63

Application	Linear Motion Shafts
Type	Shafts
Shaft Type	Shafts
System of Measurement	Inch
Material	Steel
Steel Type	AISI 1566 Steel
Finish	Plain
Surface Finish	12 rms
Hardness	Case Hardened
Minimum Hardness Depth	0.04"
Rockwell/Brinell Hardness	Rockwell C60
Outside Diameter	1/2"
Outside Diameter Tolerance	-0.0005" to -0.001"
Straightness Tolerance	0.002" per foot
Overall Length	36"
Ends	Chamfered
Material Certification	Without Material Certification
Specifications Met	American Iron and Steel Institute (AISI)
Note	Are precision ground for exacting diameter and straightness tolerances.

Application > Type > Shaft Type > Outside Diameter > Overall Length

Precision Shafts

This product matches all of your selections.

Part Number: 6061K107 $4.30 Each

Application	Linear Motion Shafts
Type	Shafts
Shaft Type	Shafts
System of Measurement	Inch
Material	Steel
Steel Type	AISI 1566 Steel
Finish	Plain
Surface Finish	12 rms
Hardness	Case Hardened
Minimum Hardness Depth	0.027"
Rockwell/Brinell Hardness	Rockwell C60
Outside Diameter	1/4"
Outside Diameter Tolerance	-0.0005" to -0.001"
Straightness Tolerance	0.002" per foot
Overall Length	10"
Ends	Chamfered
Material Certification	Without Material Certification
Specifications Met	American Iron and Steel Institute (AISI)
Note	Are precision ground for exacting diameter and straightness tolerances.

Rod Ends

This product matches all of your selections.

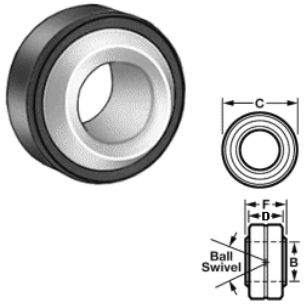

Part Number: 1071K11 $3.48 Each

Rod End Type	Ball Joint Swivel Bearings
Ball Joint Swivel Bearings Type	Ball Joint Swivel Bearings
Ball Joint Lubrication	No Lubrication Required
Bearing Housing Material	Glass-Filled Nyon
Ball Material	Nylon Composite
Race Material	Nylon Composite
Bearing Liner Material	Without Liner
Inside Diameter (B)	3/16"
Outside Diameter (C)	9/16"
Housing Thickness (D)	7/32"
Overall Thickness (F)	5/16"
Maximum Ball Swivel (23° to 35°)	34°
Temperature Range	-22° to 176° F
Static Radial Load Capacity	225 lbs.
Specifications Met	Not Rated

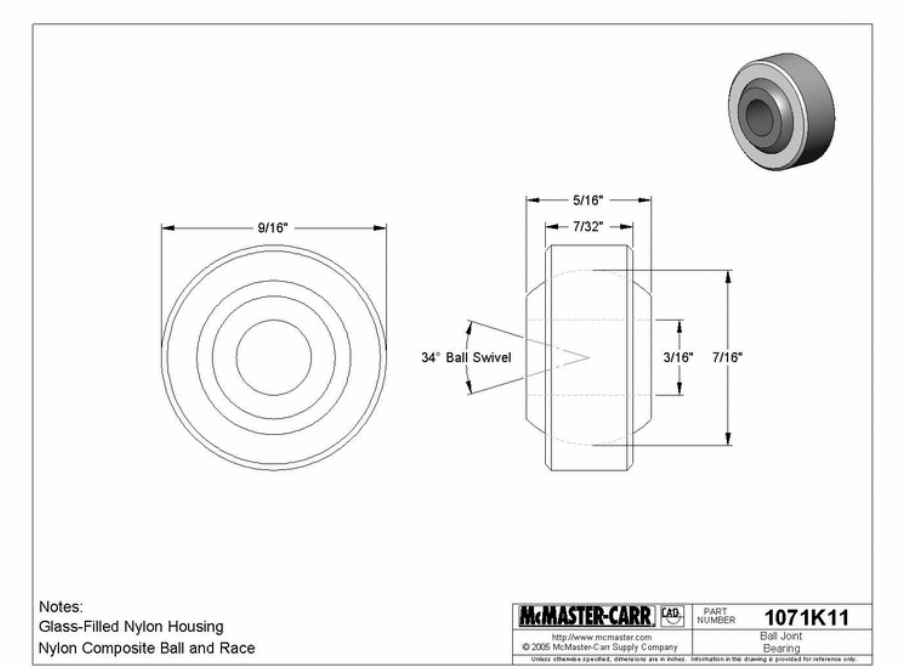

Type > Cross Section Shape > Outside Diameter > Compare Items

O-Rings, Cord Stock, and Accessories

This product matches all of your selections.

Part Number: 90025K413 — $8.13 per Pack of 10

AS568A Dash Number	340
Type	O-Ring
O-Ring Type	Standard
Cross Section Shape	Quad
Width	3/16"
Actual Width	.210"
Inside Diameter	3-3/8"
Actual Inside Diameter	3.350"
Outside Diameter	3-3/4"
Actual Outside Diameter	3.770"
Material	Buna-N
Buna-N Type	Standard
Durometer	Hard
Durometer Shore	Shore A: 70
Temperature Range	-40° to +250°F
Color	Black

vEx Microcontroller

Inputs and Outputs	
Battery input	7.2 volts nominal, 6 to 9 volts min/max input range
Battery Type	6 AA batteries (not included) or VEX Robotics Power Pack
Interrupt inputs	6
Digital I/O	16 max with no Analog, Each can be input or Output (shared with Analog)
input Impendence	Analog/Digital - The input consists of a 470K pull-up to +5V and a series resistance of 1K to the uP. Interrupts - The input consists of a series resistance of 1K to the uP. More info - input Schematic.
Analog inputs	16 max with no Digital, 10-bit resolution (shared with Digital)
Digital/Analog as inputs	3 dB bandwidth of 150 kHz, weak pull-up of 470k-ohms to 5.0 volts, need 0.0 to 0.6 volts for a low and 4.0 to 5.0 volts for a high
Interrupts as inputs	3 dB bandwidth of 150 kHz, weak pull-up of 47k-ohms to 5.0 volts, need 0.0 to 0.6 volts for a low and 4.0 to 5.0 volts for a high

Digital/Analog Interrupts as Outputs	As outputs these ports can drive an open circuit to 0.6v or lower for a low and 4.0 volts or higher for a high. They can drive a 1 mA load to 1.6v or lower for a low and 3.0 volts or higher for a high.
PWM Outputs	As outputs these ports can drive an open circuit to 0.6v or lower for a low and 4.0 volts or higher for a high. They can drive a 1 mA load to 1.0v or lower for a low and 3.6 volts or higher for a high.
Digital input Freq.	50 KHz (typical)
Analog input Access	10 µSec
Motor Output	8 PWM Outputs for motors or servos, refreshed every 18.5mSec
Serial Ports	TTL (115Kb) - Serial Port and TX/RX on Digital/Analog port
Pinout	Digital/Analog, Interrupts, Motor Outputs: Outside pin (closest to the controller edge) Ground Digital/Analog, Interrupts: Center pin (or middle pin) + 5 Volts, 1 Amp Max combined total from all pins Motor Outputs: Center pin (or middle pin) + Battery Power, 4 Amps Max combined total from all pins Digital/Analog, Interrupts, Motor Outputs: Inside pin (furthest from the controller edge) Signal / Control line
User Programmable Microcontroller	
User Microcontroller	Microchip PICmicro® PIC18F8520
Processor Speed	10 MIPS (Million Instructions Per Second)
Variable Space	1800 bytes + 1024 bytes EE2
Program Space	32K
Programming	PIC C
Programming Tools	Microchip MPLAB IDE or easyC
Erase/Write Cycles	100,000
Data Retention	> 40 years
General Features	
Size (W x L x H)	4.5" x 3.9" x 1.1"
Weight	0.28 lbs.
Battery	7.2V Rechargeable Nickel Cadmium batteries - NiCd
Charging	Recharge when battery voltage $\leq$ 7.1V, full charge 7.8V typical
Battery	7.2V Rechargeable Nickel Cadmium batteries - NiCd
Current Draw	62 mA - Controller & Receiver min, 5mA to 2A per Motor, 20mA to 1.5 A per Servo

Victor 884 Speed Controller

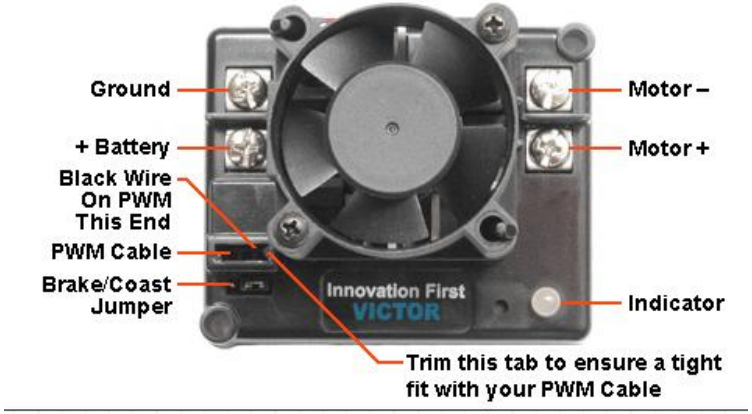

Control Signal	Standard R/C Type PWM (Pulse Width Modulation)
Operating Voltage	6V to 15V
Maximum Current	40A continuous
Minimum Throttle	3%
Power Connector	6-32 Screw Terminals
Signal Connector	Use a standard non-shrouded PWM cable (3 wires)
Typical Application	Power one motor with variable speed forward, reverse, or off
Weight	0.25 lbs

Denso Window motor

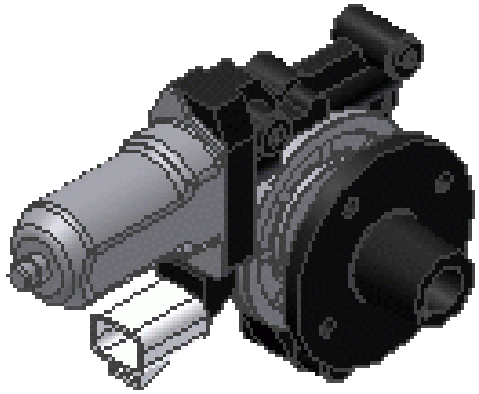

Speed (rpm)	Torque (N m)	Torque (in lbs)	Current (A)	Power (wt)	Efficiency	Heat (wt)
0	10.600	93.818	18.6	0.0	0.00%	223
6	9.893	87.560	17.5	5.9	3.00%	204
11	9.187	81.312	16.3	11.0	6.00%	185
17	8.480	75.054	15.2	15.3	8.00%	167
23	7.773	68.797	14.1	18.7	11.00%	150
29	7.067	62.548	12.9	21.2	14.00%	134
34	6.360	56.291	11.8	22.9	16.00%	119
40	5.653	50.033	10.7	23.7	19.00%	104
46	4.947	43.785	9.5	23.7	21.00%	91
52	4.240	37.527	8.4	22.9	23.00%	78
57	3.533	31.270	7.3	21.2	24.00%	66
63	2.827	25.021	6.1	18.7	25.00%	55
69	2.120	18.764	5.0	15.3	25.00%	45
75	1.413	12.506	3.9	11.0	24.00%	35
80	.707	6.257	2.7	5.9	18.00%	27
86	.000	0.000	1.6	0.0	0.00%	19

Appendix C

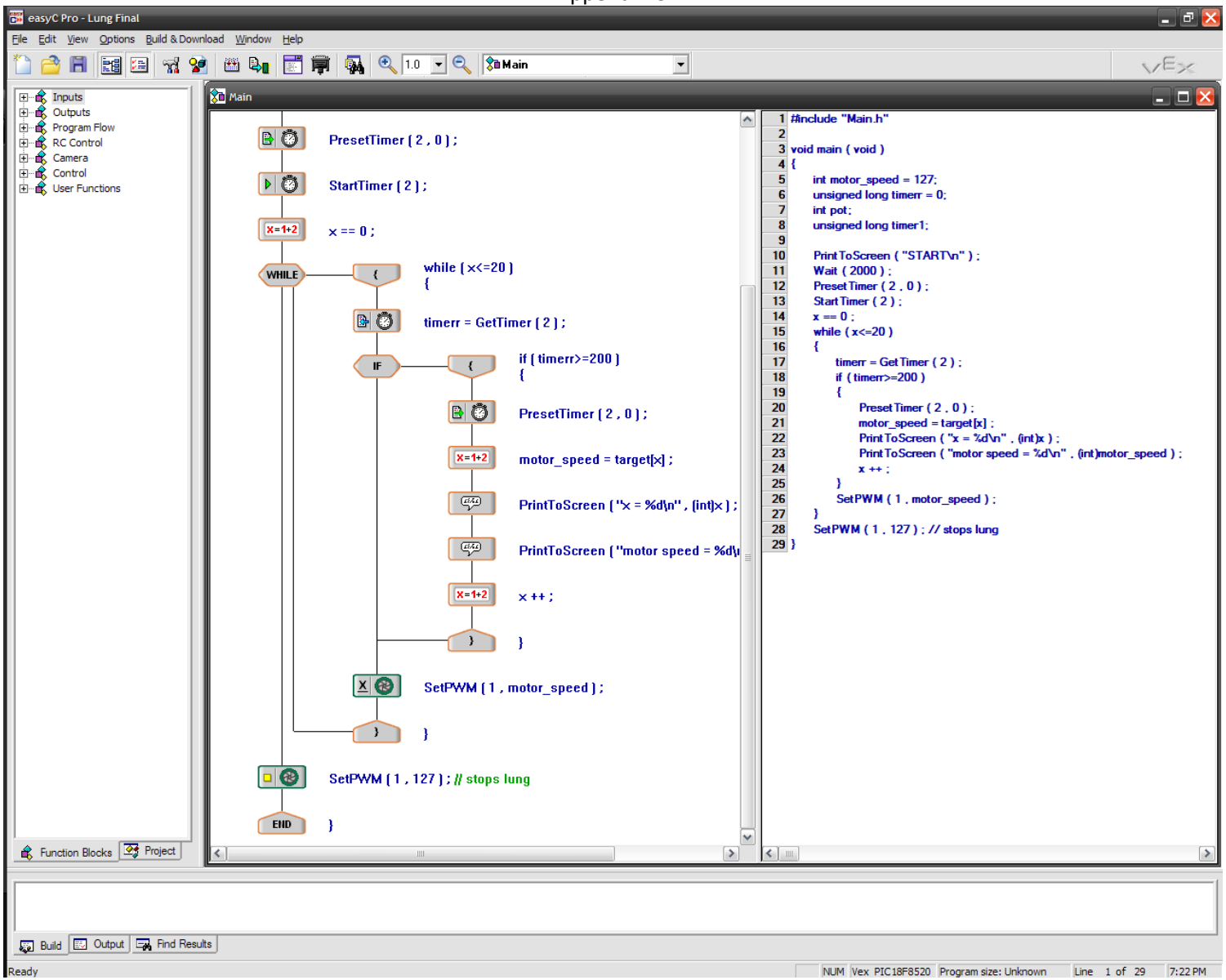
easyC Pro - Lung Final
File Edit View Options Build & Download Window Help
Main
Inputs
Outputs
Program Flow
RC Control
Camera
Control
User Functions
Function Blocks
Project
PresetTimer (2 , 0) ;
StartTimer (2) ;
x == 0 ;
while (x<=20)
{
timerr = GetTimer (2) ;
if (timerr>=200)
{
PresetTimer (2 , 0) ;
motor_speed = target[x] ;
PrintToScreen ("x = %d\n" , (int)x) ;
x ++ ;
}
SetPWM (1 , motor_speed) ;
}
SetPWM (1 , 127) ; // stops lung
}
#include "Main.h"
void main (void)
{
int motor_speed = 127;
unsigned long timerr = 0;
int pot;
unsigned long timer1;
PrintToScreen ("START\n") ;
Wait (2000) ;
PresetTimer (2 , 0) ;
StartTimer (2) ;
x == 0 ;
while (x<=20)
{
timerr = GetTimer (2) ;
if (timerr>=200)
{
PresetTimer (2 , 0) ;
motor_speed = target[x] ;
PrintToScreen ("x = %d\n" , (int)x) ;
PrintToScreen ("motor speed = %d\n" , (int)motor_speed) ;
x ++ ;
}
SetPWM (1 , motor_speed) ;
}
SetPWM (1 , 127) ; // stops lung
}
Build
Output
Find Results
Ready
NUM Vex PIC18F8520 Program size: Unknown
Line 1 of 29
7:22 PM

Appendix D

Pressure sensor voltage to mm H_2O

Voltage	Pressure (mm H_2O)	Voltage	Pressure (mm H_2O)	Voltage	Pressure (mm H_2O)
0.361	-5.098581065	0.972	-1.019716213	3.300	1.223659456
0.367	-4.996609444	1.013	-0.917744592	3.332	1.325631077
0.372	-4.894637822	1.057	-0.81577297	3.362	1.427602698
0.378	-4.792666201	1.106	-0.713801349	3.390	1.529574319
0.384	-4.69069458	1.161	-0.611829728	3.416	1.631545941
0.391	-4.588722958	1.223	-0.509858106	3.441	1.733517562
0.398	-4.486751337	1.295	-0.407886485	3.464	1.835489183
0.405	-4.384779716	1.381	-0.305914864	3.486	1.937460805
0.412	-4.282808095	1.491	-0.203943243	3.507	2.039432426
0.420	-4.180836473	1.650	-0.101971621	3.527	2.141404047
0.428	-4.078864852	1.672	-0.091774459	3.546	2.243375669
0.436	-3.976893231	1.695	-0.081577297	3.564	2.34534729
0.445	-3.874921609	1.720	-0.071380135	3.581	2.447318911
0.454	-3.772949988	1.748	-0.061182973	3.598	2.549290532
0.464	-3.670978367	1.781	-0.050985811	3.613	2.651262154
0.474	-3.569006745	1.818	-0.040788649	3.628	2.753233775
0.484	-3.467035124	1.869	-0.030591486	3.642	2.855205396
0.495	-3.365063503	1.946	-0.020394324	3.656	2.957177018
0.507	-3.263091882	2.023	-0.010197162	3.669	3.059148639
0.519	-3.16112026	2.100	0	3.681	3.16112026
0.531	-3.059148639	2.177	0.010197162	3.693	3.263091882
0.544	-2.957177018	2.254	0.020394324	3.705	3.365063503
0.558	-2.855205396	2.331	0.030591486	3.716	3.467035124
0.572	-2.753233775	2.382	0.040788649	3.726	3.569006745
0.587	-2.651262154	2.419	0.050985811	3.736	3.670978367
0.602	-2.549290532	2.452	0.061182973	3.746	3.772949988
0.619	-2.447318911	2.480	0.071380135	3.755	3.874921609
0.636	-2.34534729	2.505	0.081577297	3.764	3.976893231
0.654	-2.243375669	2.528	0.091774459	3.772	4.078864852
0.673	-2.141404047	2.550	0.101971621	3.780	4.180836473
0.693	-2.039432426	2.709	0.203943243	3.788	4.282808095
0.714	-1.937460805	2.819	0.305914864	3.795	4.384779716
0.736	-1.835489183	2.905	0.407886485	3.802	4.486751337
0.759	-1.733517562	2.977	0.509858106	3.809	4.588722958
0.784	-1.631545941	3.039	0.611829728	3.816	4.69069458
0.810	-1.529574319	3.094	0.713801349	3.822	4.792666201
0.838	-1.427602698	3.143	0.81577297	3.828	4.894637822
0.868	-1.325631077	3.187	0.917744592	3.833	4.996609444
0.900	-1.223659456	3.228	1.019716213	3.839	5.098581065
0.935	-1.121687834	3.265	1.121687834		

Pressure Sensor Output

Voltage to Pa

Figure 1:

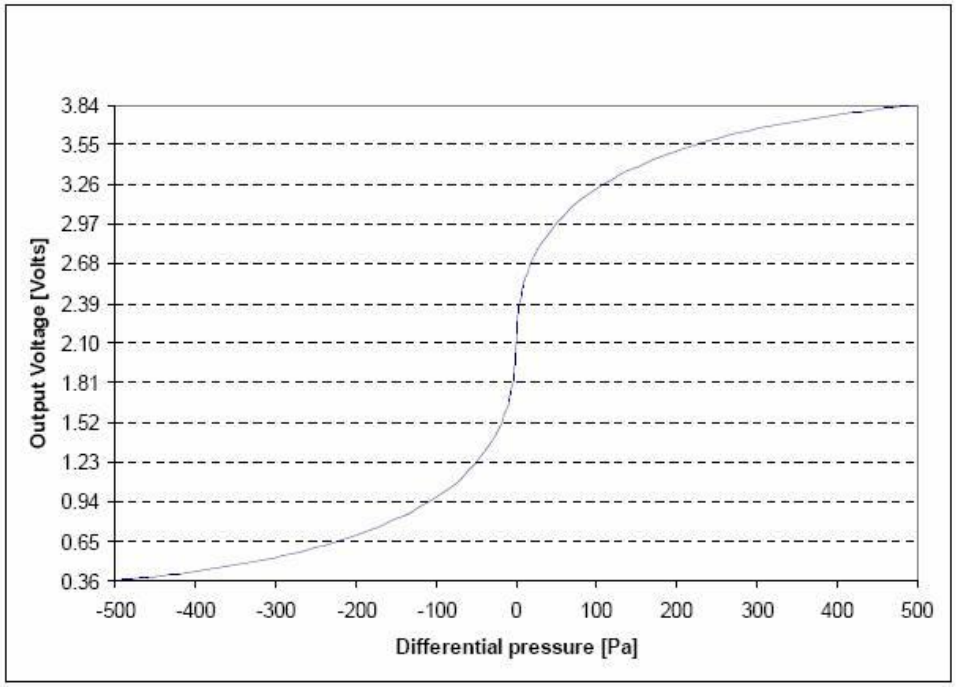

DP [Pa]	Output [Volts]	DP [Pa]	Output [Volts]	DP [Pa]	Output [Volts]	DP [Pa]	Output [Volts]	DP [Pa]	Output [Volts]	DP [Pa]	Output [Volts]
		-310	0.519	-110	0.935	0	2.100	110	3.265	310	3.681
-500	0.361	-300	0.531	-100	0.972	1	2.177	120	3.300	320	3.693
-490	0.367	-290	0.544	-90	1.013	2	2.254	130	3.332	330	3.705
-480	0.372	-280	0.558	-80	1.057	3	2.331	140	3.362	340	3.716
-470	0.378	-270	0.572	-70	1.106	4	2.382	150	3.390	350	3.726
-460	0.384	-260	0.587	-60	1.161	5	2.419	160	3.416	360	3.736
-450	0.391	-250	0.602	-50	1.223	6	2.452	170	3.441	370	3.746
-440	0.398	-240	0.619	-40	1.295	7	2.480	180	3.464	380	3.755
-430	0.405	-230	0.636	-30	1.381	8	2.505	190	3.486	390	3.764
-420	0.412	-220	0.654	-20	1.491	9	2.528	200	3.507	400	3.772
-410	0.420	-210	0.673	-10	1.650	10	2.550	210	3.527	410	3.780
-400	0.428	-200	0.693	-9	1.672	20	2.709	220	3.546	420	3.788
-390	0.436	-190	0.714	-8	1.695	30	2.819	230	3.564	430	3.795
-380	0.445	-180	0.736	-7	1.720	40	2.905	240	3.581	440	3.802
-370	0.454	-170	0.759	-6	1.748	50	2.977	250	3.598	450	3.809
-360	0.464	-160	0.784	-5	1.781	60	3.039	260	3.613	460	3.816
-350	0.474	-150	0.810	-4	1.818	70	3.094	270	3.628	470	3.822
-340	0.484	-140	0.838	-3	1.869	80	3.143	280	3.642	480	3.828
-330	0.495	-130	0.868	-2	1.946	90	3.187	290	3.656	490	3.833
-320	0.507	-120	0.900	-1	2.023	100	3.228	300	3.669	500	3.839

voltage output under calibration conditions (23°C and $p_{absolute}$ = 966 mbar, dry air, V_{DD} = 5.0 V)

Appendix E

Software Instructions.

1) Open the easy c program titled Final Lung which is contained on the disk provided with this paper.

2) Click on the Build and Download tab then select On-Line Window…

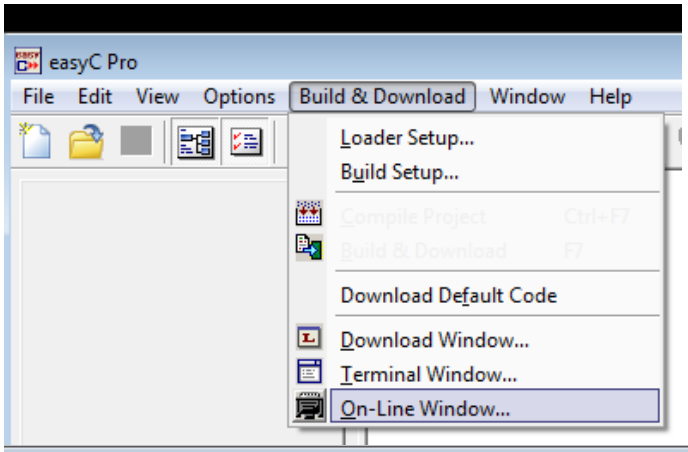

3) In this window the scotch yoke arm may be adjusted into the initial arm position through the use of the motor control slider #1 pictured to the right. The arm should be parallel to the guide rails with the piston in the forward most position. Close the on-line window.

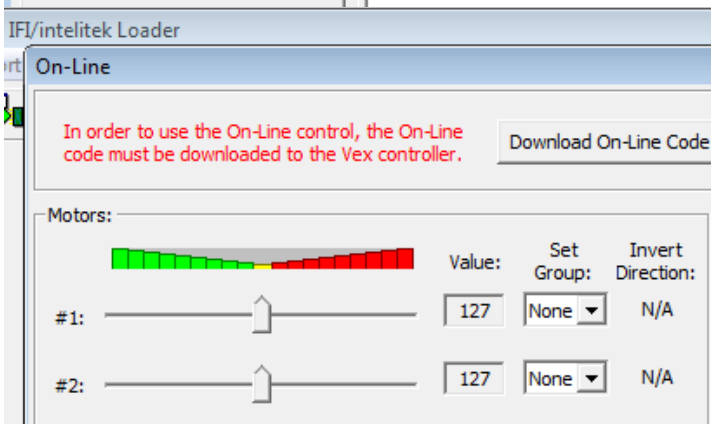

4) Now open up the file LABVIEW.VI found in the folder “Use This Labview” contained on the disk provided with this paper. It should look like the VI to the right.

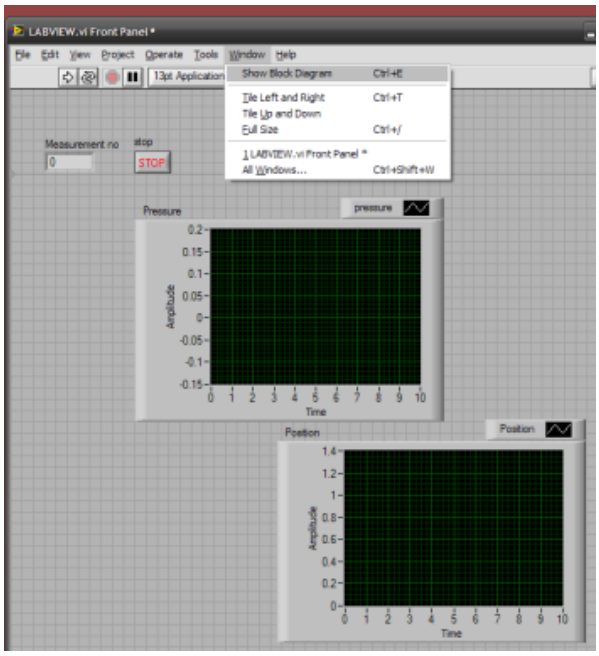

5) Click on the Window Tab and then select Show Block Diagram

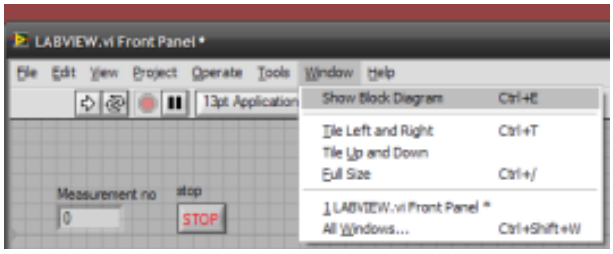

6) From this screen you should double click on the Write to Measurement File

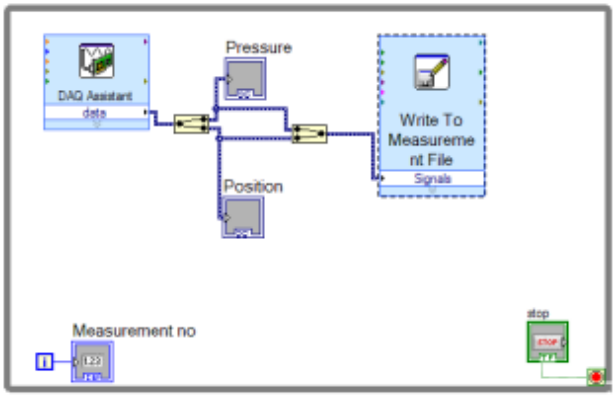

7) Click on the folder icon shown to the right and browse to your location of choice for the data output.
Close this window and the Block Diagram.
Run the VI and look to see that data was written to the specified location.

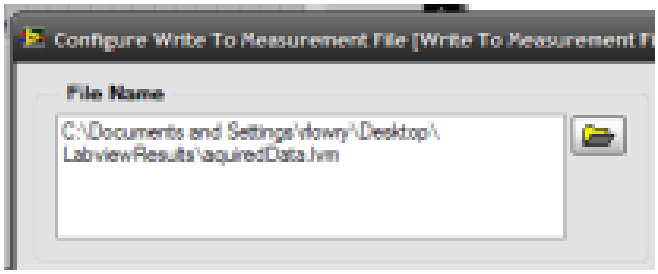

8) Move back to easy C, click the Build and Download drop down menu and select Build and Download.

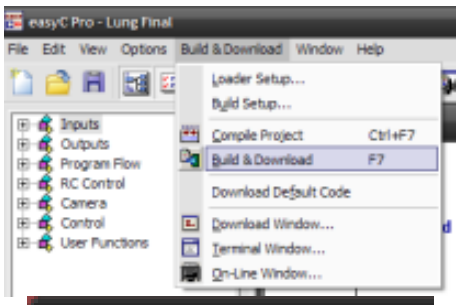

9) Once the code has downloaded to the controller there are only two seconds until the lung starts to move. The run button on the LabView VI needs to be hit during this time.

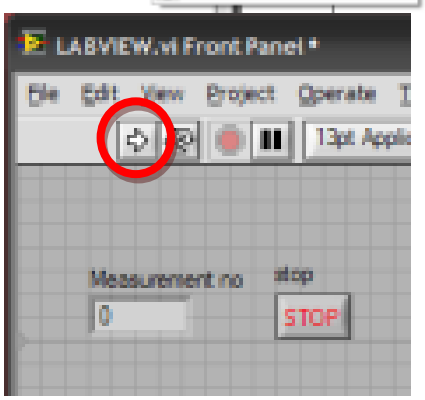

10) Once the arm has completed one rotation stop the Labview VI using the STOP button shown previously next to the Measurement no. indicator. The results excel sheet should look like the one to the right.

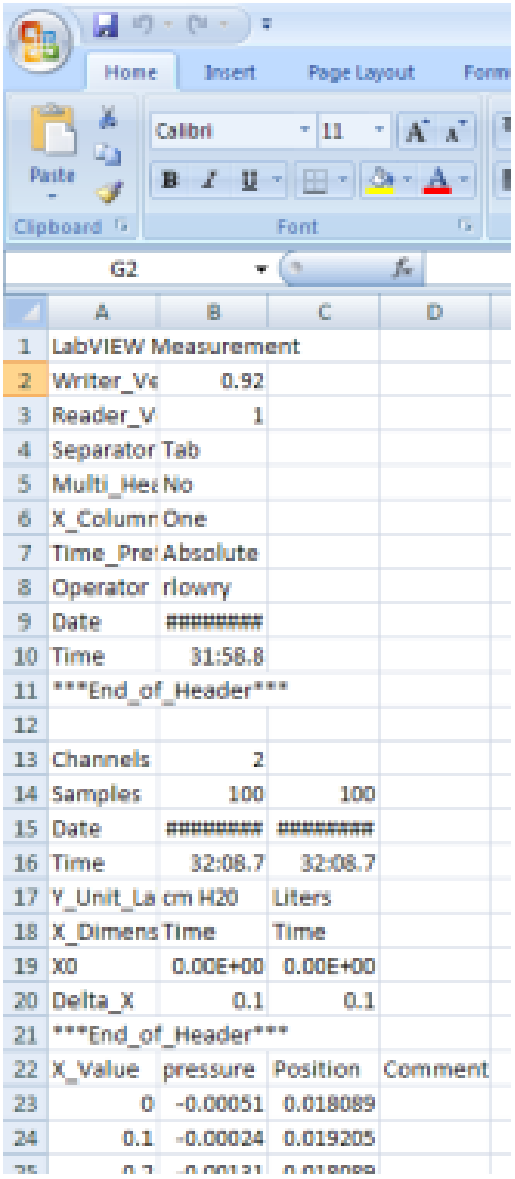

	A	B	C	D
1	LabVIEW Measurement			
2	Writer_Ve	0.92		
3	Reader_V	1		
4	Separator	Tab		
5	Multi_Hea	No		
6	X_Columr	One		
7	Time_Pre	Absolute		
8	Operator	rlowry		
9	Date	########		
10	Time	31:58.8		
11	***End_of_Header***			
12				
13	Channels	2		
14	Samples	100	100	
15	Date	#########	#########	
16	Time	32:08.7	32:08.7	
17	Y_Unit_La	cm H20	Liters	
18	X_Dimens	Time	Time	
19	X0	0.00E+00	0.00E+00	
20	Delta_X	0.1	0.1	
21	***End_of_Header***			
22	X_Value	pressure	Position	Comment
23	0	-0.00051	0.018089	
24	0.1	-0.00024	0.019205	

11) Start selecting Data where you can see the lung volume changing from its initial value and highlight the values for 4 seconds after this time.
The pressure readings are given in cm of H20 and the volumes are given in Liters.

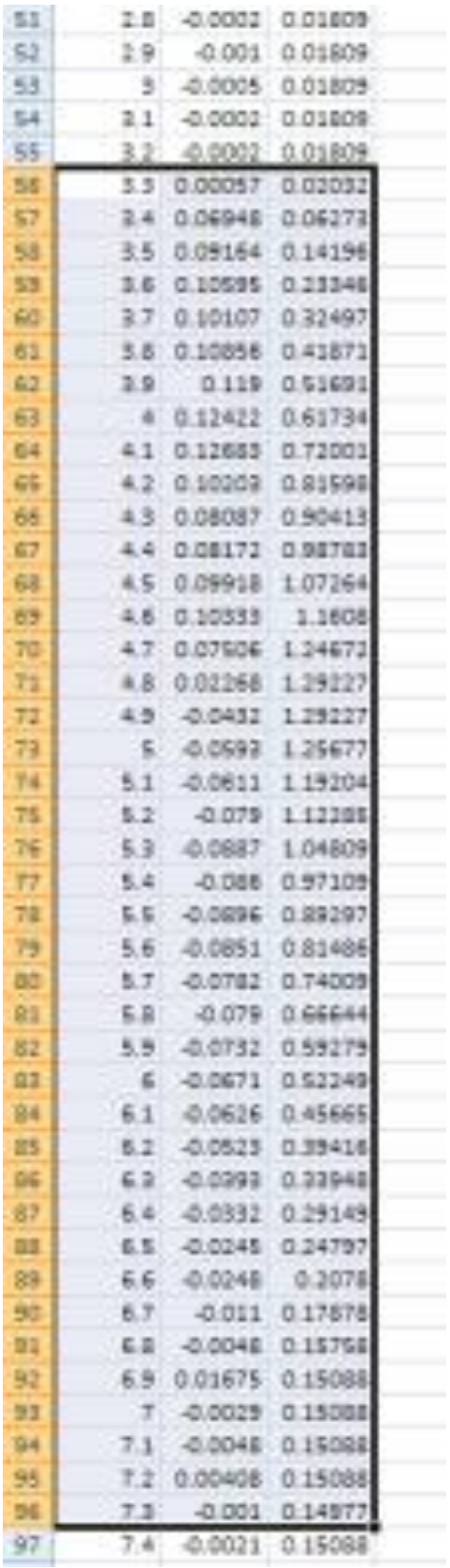

51	2.8	-0.0002	0.01809
52	2.9	-0.001	0.01809
53	3	-0.0005	0.01809
54	3.1	-0.0002	0.01809
55	3.2	-0.0002	0.01809
56	3.3	0.00057	0.02032
57	3.4	0.06948	0.08273
58	3.5	0.09164	0.14196
59	3.6	0.10595	0.23348
60	3.7	0.10107	0.32497
61	3.8	0.10856	0.41871
62	3.9	0.119	0.51691
63	4	0.12422	0.61734
64	4.1	0.12683	0.72001
65	4.2	0.10203	0.81598
66	4.3	0.08087	0.90413
67	4.4	0.08172	0.98783
68	4.5	0.09918	1.07264
69	4.6	0.10533	1.1608
70	4.7	0.07606	1.24473
71	4.8	0.02268	1.29127
72	4.9	-0.0431	1.29127
73	5	-0.0593	1.25677
74	5.1	-0.0611	1.19204
75	5.2	-0.079	1.12288
76	5.3	-0.0687	1.04809
77	5.4	-0.088	0.97109
78	5.5	-0.0896	0.88297
79	5.6	-0.0851	0.81486
80	5.7	-0.0782	0.74009
81	5.8	-0.079	0.66644
82	5.9	-0.0732	0.59279
83	6	-0.0671	0.52248
84	6.1	-0.0626	0.45665
85	6.2	-0.0523	0.39416
86	6.3	-0.0393	0.33948
87	6.4	-0.0332	0.29149
88	6.5	-0.0245	0.24797
89	6.6	-0.0248	0.2078
90	6.7	-0.011	0.17678
91	6.8	-0.0048	0.15768
92	6.9	0.01675	0.15088
93	7	-0.0029	0.15088
94	7.1	-0.0048	0.15088
95	7.2	0.00408	0.15088
96	7.3	-0.001	0.14877
97	7.4	-0.0021	0.15088

12) This data may either be pasted into the File Data for final paper by placing the cursor as shown to the left. This allows for comparison of the recorded data against other trials and the given data. You may also paste the data into program for analysis.
The LabView VI will automatically overwrite the acquired data file when it is run again.

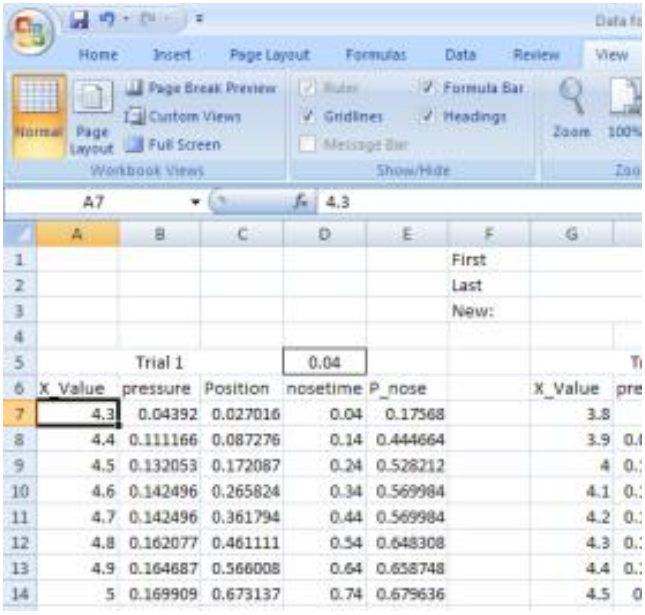

	A	B	C	D	E	F	G
1						First	
2						Last	
3						New:	
4							
5		Trial 1		0.04			
6	X_Value	pressure	Position	nosetime	P_nose		X_Value
7	4.3	0.04392	0.027016	0.04	0.17568		3.8
8	4.4	0.111166	0.087276	0.14	0.444664		3.9
9	4.5	0.132053	0.172087	0.24	0.528212		4
10	4.6	0.142496	0.265824	0.34	0.569984		4.1
11	4.7	0.142496	0.361794	0.44	0.569984		4.2
12	4.8	0.162077	0.461111	0.54	0.648308		4.3
13	4.9	0.164687	0.566008	0.64	0.658748		4.4
14	5	0.169909	0.673137	0.74	0.679636		4.5

13) Repeat steps 2 and 3 again if necessary to reposition the arm and then steps 8 through 11 for each successive trial.